UNIVERSITY OF COPENHAGEN

Master's thesis

Electronic transport properties in Pb-based hybrid nanowire devices

Author:
Yan Chen

Supervisors:
Peter Krogstrup
Yu Liu

Center for Quantum Devices
Niels Bohr Institute

August, 2021

Abstract

This thesis explores the electronic properties of hybrid semiconductor-superconductor nanowires which hold promise as a material platform to realize topologically protected Majorana quasi-particles. The development of epitaxial materials that exhibits large superconducting hard gap is one of the key directions in this field. Here, we are considering Pb-based materials. The InSb and InAsSb semiconductor nanowires with strong spin-orbit interaction and large Landé-g factor were grown using molecular beam epitaxy. The Pb superconducting film was deposited on the side facets of the nanowires in-situ after the nanowire growth. The devices were fabricated and then characterized electrically at low temperatures. Pb shows normal superconducting transition at critical temperature (7.0K) and critical magnetic field (1.14T) at 1.7 K. When $T = 0$,the critical field $H_c(0)$ is estimated to be 1.27 T. Then, for InSb/Pb nanowire which is half shell, the pinch off behavior was observed, and for InAsSb/Pb nanowire with shadow junctions, the conductance of quantization behavior at high magnetic fields were realized.

Acknowledgements

I would like to extend my gratitude to Peter Krogstrup for accepting me into his group. Investigating materials is such an interesting and great work. Thanks to him, I could get close to this field and know the frontier of materials research. My special thanks to Yu Liu for guiding and teaching me how to write a formal thesis. His patience with me is so great gift for me on this project. Harry Charalampos Lampadaris, Sabbir A. Khan, thank you, without your help, I could not deal with the device design and fabrication problems and all other problems I faced when I were doing experiments. Besides, I also want to say thank you to Cui Ajuan, Nikhil Niranjan Maka Jung-hyun (Jordan) Kang for giving me many suggestions in this journey. Many thanks to all of you.

Contents

Chapter 1 Motivation and introduction

1.1 Topology and Majorana bound state

In 2016, David J. Thouless, F. Duncan M. Haldane, J. Michael Kosterlitz won the Noble Prize in Physics for discovering that even microscopic matter could exhibit macroscopic properties and phases which are topological [1]. First of all, topology [2] is a branch of mathematics that focuses on fundamental properties of objects. This property of a geometric object would be preserved when the object is gradually bent or stretched. For instance, in the Figure 1.1, a donut and a cup look as one based on the topological properties because they both have one hole. You could reshape a donut into a cup under continuous deformations. However, a pretzel that has three holes is different from a donut because there are no smooth incremental changes that turn a donut into a pretzel.

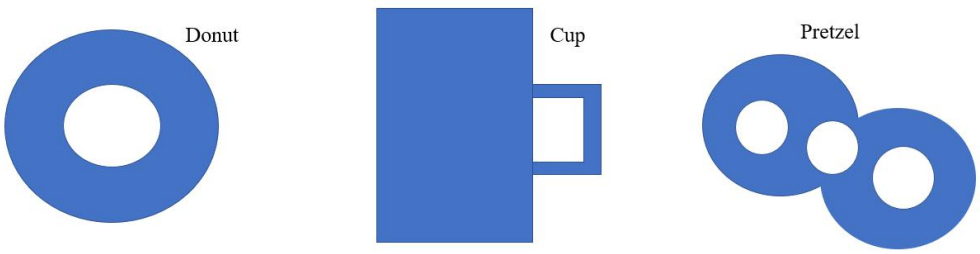

Figure 1.1: Examples of objects to show topology. A donut and a cup are the same because they both have one hole. A donut could change into a cup smoothly. However, a donut could not turn into a pretzel because the pretzel has three holes. There are no smooth incremental changes between them.

Then the Nobel laureates, David J. Thouless, F. Duncan M. Haldane, J. Michael Kosterlitz, discovered that the topological properties exist at the quantum level. And the discovery has

revolutionized materials science, electronic engineering, and computer science. Materials exhibiting topological phases and properties include superconductors with strong spin-orbit coupling[3], topological insulators[4], and Weyl and Dirac semimetals[5].

From definition in particle physics, Majorana fermion [6] is a fermion that is its own anti-particle, which was proposed by Ettore Majorana in 1937 when he was solving the Dirac equation. So far, no particle meets this requirement as to be identical to its anti-particle in nature yet. The neutrino was supposed to be Majorana fermion, but the possibility was then excluded in the experimental discoveries. The concept of Majorana fermions is borrowed in condensed matter system as Majorana quasiparticles, which have potential to achieve fault-tolerant quantum computing. A fermionic state can be obtained as a superposition of two Majorana fermions $f = \gamma_1 + \mathrm{i}\,\gamma_2$. Each of them is split into a real and imaginary part of a fermion.

The p-wave superconductors are predicted to create Majorana-type excitations [3]. They can contain magnetic flux (vortices) that could trap so-called zero modes, which are spin $1/2$ excitons combined with electrons ("filled") and holes ("empty") with zero energy. These zero modes are created by the creation operator c_j^+ for particle states (electron) and its conjugate operator c_j for anti-particles (hole) states [7]

$$\gamma_j = c_j^+ + c_j \tag{1.1}$$

They are called Majorana zero modes (MZMs) (or Majorana bound state, Majorana quasiparticle) that are able to act as Majorana fermion. Each of them is split into a real and imaginary part of a fermion so that it is spatially non-local and has a long coherence time.

Due to the characteristics of Majorana fermions, the p-wave superconductors have great potential for building quantum computers. Quantum computer takes advantage of the fact the

subatomic particles can be in different states namely to store information in something called quantum bits or qubits, which are expecting to solve problems exponentially faster than the classical computer. But this process is so sensitive that its interaction with the environment could easily destroy itself. Meanwhile, in topological phases, particles can become protected, which means the qubits form by these phases can't be destroyed by local or small disturbances, so the topological qubits would be more stable, resulting in a better quantum computer.

1.2 Searching for Majorana zero modes

I) Hybrid semiconductor-superconductor nanowire (NW)

Proposed by Kitaev et. al. [8], the MZMs are expected to appear in a pair at the edge of a one-dimensional spinless p-wave superconductor although it does not exist in a natural state. Instead of there is a semiconductor with strong spin-orbit interaction proximitizedly coupling to a conventional superconductor, it is expected to realize MZMs because the hybrid system could function as a spinless p-wave superconductor [9]. Therefore, the study of hybrid semiconductor-superconductor nanowires has attracted huge interests recently.

More specifically, in order to enter topological states, the hybrid structures should meet the requirements as follows:

1. Conventional s-wave superconductivity

   The particle-hole symmetry from superconductivity would create a level of zero energy which can be therefore topologically protected. It is important to have a high interface quality between superconductor and semiconductor.

2. Magnetic fields

   With a magnetic field perpendicular to the direction of the spin–orbit coupling the system could open a gap at $k = 0$. It removes the spin degeneracy, leading to the

completely spin-less 1-D system. The expression of the energy gap at $k = 0$ can be written as

$$E_G = \left| E_z - \sqrt{\Delta^2 + \mu^2} \right| \tag{1.2}$$

$E_z = g\mu_B B$,where g is the Landé-g factor factor and μ_B is the Bohr magneton. Δ is the superconducting gap. If the applying magnetic field is increasing until it is higher than the superconducting gap, $E_z > \sqrt{\Delta^2 + \mu^2}$, it will result into the emergence of spin-less superconductivity. Therefore, by changing magnetic field or Zeeman coupling E_z as shown in Figure 1.2e, the system could be driven into topological phase [10]. The valve of chemical potential μ would also affect the appearance of this phase.

3. Semiconductor with strong spin-orbit interaction and thus a large Landé-g factor

Based on the above analysis, it is found that the Landé-g factor also have contribution to the Zeeman coupling E_z. Therefore, the semiconductors with large Landé-g factors can reduce the required magnitude of magnetic fields for the system to enter topological states. So we are focusing on semiconductors such as InAsSb and InSb.

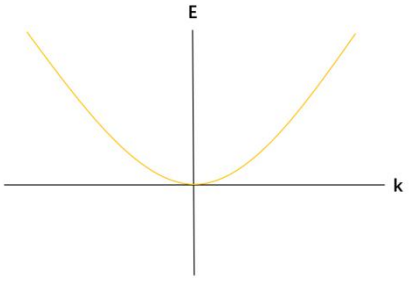

a) $\Delta = 0, \mathrm{E_z} = 0, \mathrm{SOI} = 0$

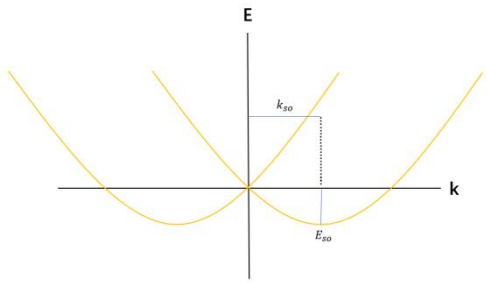

b) $\Delta = 0, \mathrm{E_z} = 0, \mathrm{SOI} > 0$

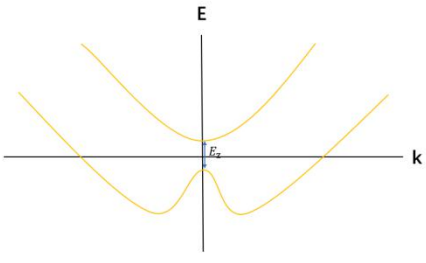

c) $\Delta = 0, \mathrm{E_z} > 0, \mathrm{SOI} > 0$

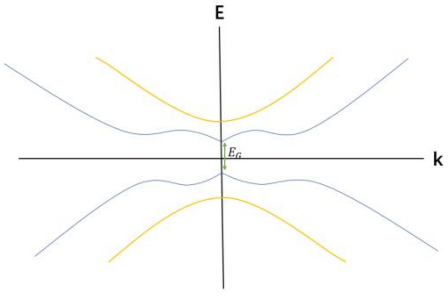

d) $\Delta > 0, \mathrm{E_z} > 0, \mathrm{SOI} > 0$

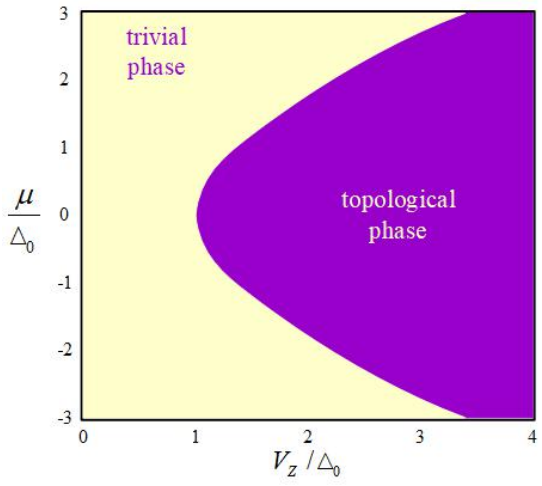

e

Figure 1.2: Energy spectrum of one-dimensional hybrid nanowire. a) Energy spectrum as a function of the momentum, which are doubly spin degenerate. **b)** Spin-orbit coupling is introduced into the system. It shift this parabolas by k_{so}, and introduce the new energy scale E_{so}. **c)** Magnetic field is applying to the system. It opens a Zeeman coupling E_z at $k = 0$. **d)** Proximity-induced superconductivity in the system. A superconducting gap Δ is open. The Zeeman coupling is larger than the superconducting gap $E_z > \Delta$, where the a topological phase will be introduced. **e)** Topological quantum phase diagram in Ref..[10]. When the Zeeman coupling is larger than the superconducting gap $E_z > \Delta$, the topological phase is shown in the blue region, which is dependent of the valve of chemical potential μ and the Zeeman coupling E_z.

Under the guidance of the above theoretical research, searching Majorana quasiparticles experimentally in the superconductor-semiconductor nanowire composite systems has become a hot topic in condensed matter physics. In fact, before Majorana quasiparticle theory, there have been many experimental studies on semiconductor nanowires with spin orbit interaction. The electron transport measurement of InAs and InSb nanowires shows that they have strong spin orbit interaction, high g-factor, high mobility materials [11], and they can form a good coupling with superconductors [12].

Scientists are producing and studying various solid state systems that conform to the proposal in order to find Majorana zero modes in the past ten years. Majorana zero modes can be

detected in the tunneling conductance as a zero bias peak (ZBP) or zero energy conductance peak, though this peak may also come from other physics, including Kondo effects [13] and weak-antilocalization [14], so distinguishing the state is topological or not is also important. The first zero bias peak signature was report in Ref.[15] in 2012. They used InSb nanowires contacted with one superconducting electrode (NbTiN) to build hybrid semiconductor-superconductor devices (Figure 1.3). Similar signatures were also found later in Nb-InSb[16], Al-InAs[17] and other systems [18] [19] [20].

However, there are two significant differences between the theoretically predicted Majorana zero energy conductance peak and the experimentally detected zero energy conductance peak. One is that the theoretically predicted zero energy conductance peak induced by Majorana quasiparticles is in the energy gap formed by the superconductor, but the signal obtained in the experiment is accompanied by many impurity states. For instance, non-zero sub-gap conductance and so called soft-gap problem would appear inevitably. Soft-gap problem is caused by the interface inhomogeneities mainly. To solve the problem and observe the hard-gap Majorana, it is important to improve the quality of semiconductor-superconductor interface. Second is that the Andreev reflection process caused by the Majorana quasiparticles has perfect particle-hole symmetry. Because of that, the conductance peak caused by it should be quantized and show a valve of $\frac{2e^2}{h}$, but the peak observed in the experiment did not appear this behavior. In order to solve the inconsistency between these theories and experiments, the optimization of the preparation process of materials and devices in the experiment became the key point. Then the in-situ semiconductor-superconductor growth reported in Ref.[21] in 2015 made great breakthrough. Al is directly grown on InAs nanowrie with breaking the vacuum in this report, and it avoids surface oxidization problem which would damage the interface.

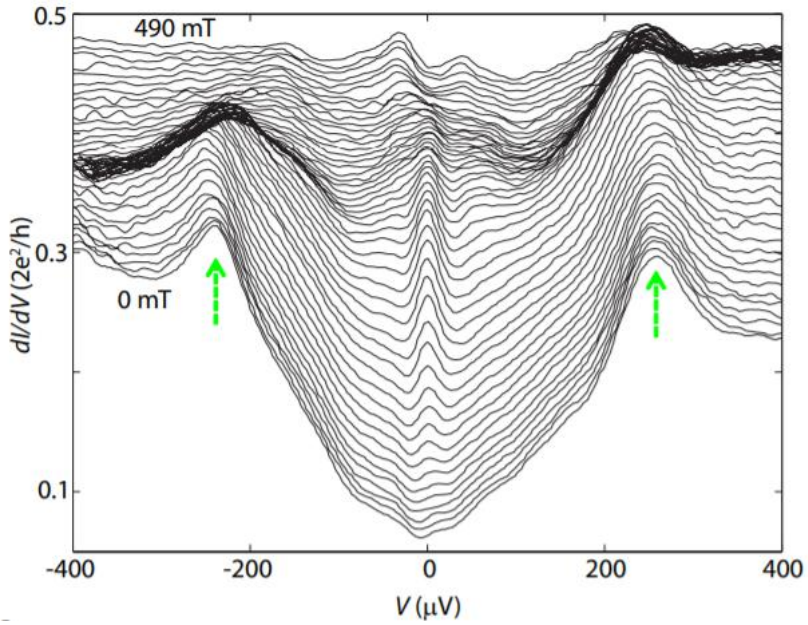

Figure 1.3: Tunneling conductance spectrum of an NbTiNb-InSb nanowire. Date is from Ref.[15]

InAs/Al

As mentioned above, the first in-situ semiconductor-superconductor growth method was introduced with InAs/Al [21]. It is an excellent material combination for topological hybrid semiconductor-superconductor quantum devices. On one hand, InAs has a strong spin orbit coupling and a large g-factor that meet the requirement of the proposal. On the other hand, Al has a long superconducting coherence length and is compatible with the standard device fabrication process. In 2015, Krogstrup et al. [21] presented great epitaxial growth of semiconductor-metal core-shell nanowires by molecular beam epitaxy (MBE). Similar to the discussion in Chapter 3 in the following, the standard in situ Au assisted nanowire growth process was used. It showed highly order epitaxial superconductor-semiconductor interfaces. The large sub-gap conductance due to the disorder at the semiconductor-superconductor interface, which will degrade topological protection, could be suppressed. Compared with the gap of the evaporated superconductor nanowire devices in the early years, these high quality epitaxial semiconductor-superconductor interfaces have been proved to show a much harder gap, which is reported in Ref.[22]. What's more, Khan et al. [23] reported the epitaxy of

semiconductor-superconductor shadow junctions nanowires that would make less disorder in junctions.

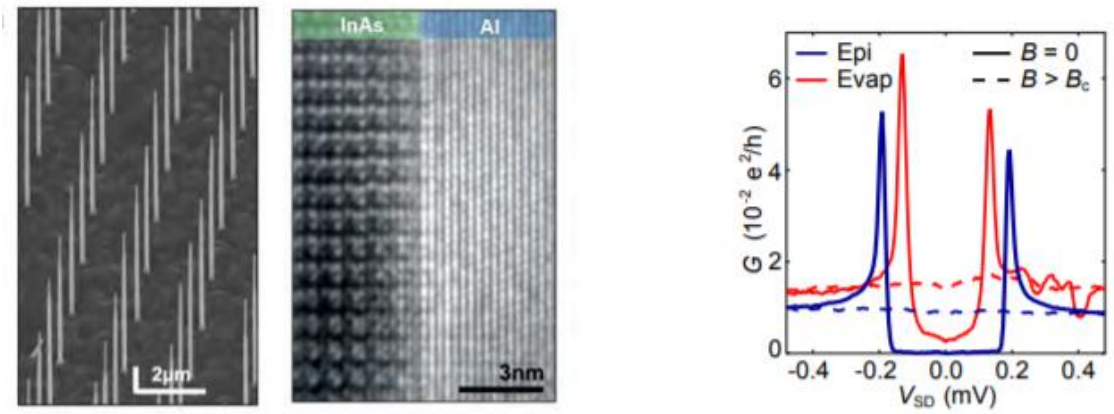

Figure 1.4: Epitaxial InAs/Al hybrids from Ref.[21] and Ref.[22]. a) Top view of scanning electron micrograph (SEM) of an array of epitaxial InAs/Al nanowires. **b)** Transmission electron microscope (TEM) micrograph of the InAs/Al nanowires. **c)** Gap hardness comparison between evaporated InAs/Al hybrid nanowire and epitaxial grown InAs/Al hybrid nanowire

InSb/Al

InSb nanowires are also great candidate for Majorana devices due to its ultra-strong spin-orbit interaction and large g-factor. InAs nanowires exhibit wurtzite (WZ) crystal structure, and InSb nanowires exhibit zincblende (ZB) crystal structure. InSb nanowires thus show ballistic transport even in zero magnetic field reported in Ref.[24]. A group in Delft [25] proposed the epitaxy of InSb nanowire networks with Al islands covered. Hard gap can also be found in the system. Additionally, Majorana zero modes were kind of observed in InSb/Al system according to Ref.[26], but it is now still unconvincing.

Other materials: InAsSb/Al, InAs/Al/EuS

$InAs_{1-x}Sb_x$ nanowires are predicted to exhibit strongest spin-orbit interaction compared with InAs and InSb [27]. Report in Ref.[28] presented the hybrid epitaxial InAsSb/Al nanowire materials, and they could also allow for a hard superconducting gap.

As the proposal said, we need to induce Zeeman splitting in the hybrid semiconductor-superconductor. Besides applying an externally magnetic field, the proximity effect from ferromagnetic insulators can also induce Zeeman splitting. InAs/EuS/Al was also been reported to have zero-bias conductance peaks with an inferred remanent Zeeman field of ~ 1.3 T [29].

Different superconductors: InAs/Pb, InAs/Sn

Besides providing stronger spin-orbit interaction, larger gap epitaxial shell nanowires are also needed to be considered and investigated. Pb and Sn currently are reported to grown on InAs nanowires [30] and InSb nanowires [31] respectively. They both yields hard induced superconducting energy gaps, and 2e transport in Coulomb charging experiments which are crucial features for topological states.

II) Other systems

There are also other proposals that are expected to hold Majorana bound states besides the hybrid semiconductor-superconductor nanowire devices. Ferromagnetic iron (Fe) atomic chains is placed in proximity to a conventional superconductor (Pb) was also to reported to show zero bias peak features according to the Ref.[32], which could achieve spatial and spectral resolution when detecting Majorana bound states. Majorana bound states were also detected in an iron-based superconductor system. In 2018, a group in China reported that Majorana bound states could be discovered in the bulk superconductor $FeTe_{0.55}Se_{0.45}$, using high-resolution scanning tunneling microscopy/spectroscopy (STM/S) experiment[33].

III) Materials in this thesis

This thesis is considering Qdev999 InSb/Pb and Qdev996 InAsSb/Pb. As mentioned above, InAsSb and InSb with large g-factors would bring down the required external magnetic field to introduce topological phase, so they are perfect semiconductor candidates. So far they have been studying for many years [24-28] which I have given a short introduction in the Section 1.2. On the other hand, Kanne et al. [30] have observed zero-field 2e periodic transport and bound-state-induced 1e periodic transport in InAs/Pb island devices but no topological superconductivity has ever been reported in Pb-based system. Compared with Al which has been studying for years [21-29], Pb is still a new material for exploration. Pb has a higher transition temperature, a higher critical magnetic field, and a larger induced superconducting energy gap. It is interesting to broaden the list of candidate material which would give much more potential to introduce and study MZMs.

In this work we will study Pb-based InSb or InAsSb VLS nanowires grown by vapour–liquid–solid mechanism. We investigated the semi-conductivity and superconductivity in InSb/Pb nanowires. To obtain InSb/Pb nanowires with in-situ junctions, 30% Sb was replaced by As to increase the yield of growth. We further studied these InAsSb/Pb nanowires with shadow junctions.

1.3 Outline

The chapters outlines are the following:

Chapter 2 introduces the basic theory of nanowires (Qdev999 InSb/Pb and Qdev996 InAsSb/Pb) that we are investigating. The epitaxy of VLS hybird nanowires would be reported. Next, the theoretical background of superconductor and semiconductor is introduced.

Chapter 3 introduces growth process first, and then the device fabrication and experimental setup we use. We discuss how to make devices for the further measurement. And the low temperature measurement setup, Physical Property Measurement System (PPMS) is presented.

Chapter 4 reports the results during the low temperature measurement. Both InSb/Pb (Qdev999) and InAsSb/Pb (Qdev996) will be concerned. We will discuss their both performances on superconductor and semiconductor at low temperature.

Chapter 5 concludes the experiment findings and provides the outlook regarding the future work.

Chapter 2 Theory

In order to comprehend the work, it is also important to have a basic knowledge of some physical concepts. This chapter will introduce the general theories about superconductor and semiconductor.

2.1 Superconductivity

Basic phenomena of superconductivity

Superconductivity is a set of physical properties observed in certain materials where electrical resistance vanishes and magnetic flux fields are expelled from the material [34]. The resistance of superconductors will disappear completely when the temperature is below a critical temperature Tc. Due to the complete disappearance of resistance, the superconducting current can be persistent for a long time without measurable decay.

The Meissner effect [35] (or Meissner–Ochsenfeld effect) is the expulsion of a magnetic field from a superconductor during its transition to the superconducting state when it is cooled below the critical temperature. This expulsion will repel a nearby magnet. Meissner effect implies that superconductivity will be destroyed by a critical magnetic field H_c. which is related thermodynamically to the free-energy difference between the normal and superconducting state. It can be described as:

$$\frac{H_c^2(T)}{8\pi} = C_n(T) - C_s(T) \tag{2.1}$$

where C_n and C_s are the zero-field Helmholtz free energies per unit volume in the normal and superconducting states.

The critical field can be approximated by a parabolic law:

$$H_c(T) = H_c(0)\left[1 - \left(\frac{T}{T_c}\right)^2\right] \tag{2.2}$$

London equations

The London equations[36], developed by brothers Fritz and Heinz London in 1935, are constitutive relations for a superconductor relating its superconducting current to electromagnetic fields in and around it. There are two London equations when expressed in terms of measurable fields:

$$\frac{\partial \mathbf{j}_s}{\partial t} = \frac{n_s e^2}{m}\mathbf{E}, \qquad \nabla \times \mathbf{j}_s = -\frac{n_s e^2}{m}\mathbf{B}. \tag{2.3}$$

In superconductors, the London penetration depth λ_L characterizes the distance to which a magnetic field penetrates into a superconductor and becomes equal to e^{-1} times that of the magnetic field at the surface of the superconductor. Therefore, when considering a superconductor within free space where the magnetic field outside the superconductor is a constant value pointed parallel to the superconducting boundary plane in the z direction, if x leads perpendicular to the boundary, then the solution inside the superconductor may be shown to be:

$$B_z(x) = B_0 e^{-x/\lambda_L} \tag{2.4}$$

While $\lambda_L(0)$ at 0 K is:

$$\lambda_L(0) = \left(\frac{mc^2}{4\pi n_s e^2}\right)^{1/2} \tag{2.5}$$

Where m is the mass of electron, e is the charge of electron, n_s is the superconducting carrier density, which is no more than the density of conduction carriers. Here, we can see the London penetration depth is closely related with the superconducting carrier density.

Ginzburg Landau theory

Based on Landau's previously established theory of second-order phase transitions, Ginzburg and Landau [37] argued that the superconducting phase can be characterized by a complex order parameter Ψ(r). It is zero when it is in metallic phase which is above T_c, and it is finite in the superconducting phase. This order parameter Ψ(r) can be regarded as the wave-function describing the centre of mass motion of a Cooper pair according to the BCS theory. The Ginzburg–Landau equations thus are:

$$\begin{aligned} &\alpha\psi + \beta|\psi|^2\psi + \frac{1}{2m}(-i\hbar\nabla - 2e\mathbf{A})^2\psi = 0 \\ &\nabla \times \mathbf{B} = \mu_0\mathbf{j} \;\; ; \;\; \mathbf{j} = \frac{2e}{m}\,\mathrm{Re}\{\psi^*\,(-i\hbar\nabla - 2e\mathbf{A})\,\psi\} \end{aligned} \tag{2.6}$$

The Ginzburg–Landau equations predicted two new characteristic lengths in a superconductor. The first characteristic length was termed coherence length ξ. For T > Tc (normal phase), it is given by:

$$\xi = \sqrt{\frac{\hbar^2}{2m|\alpha|}} \tag{2.7}$$

While for $T < T_c$ (superconducting phase), where it is more relevant, it is given by:

$$\xi = \sqrt{\frac{\hbar^2}{4m|\alpha|}} \tag{2.8}$$

The second one is the penetration depth λ, which has been introduced in London theory.

The ratio κ = λ/ξ is presently known as the Ginzburg–Landau parameter. Type I superconductors are those with $0 < \kappa < 1/\sqrt{2}$, and Type II superconductors those with $\kappa > 1/\sqrt{2}$ (Figure 2.1).

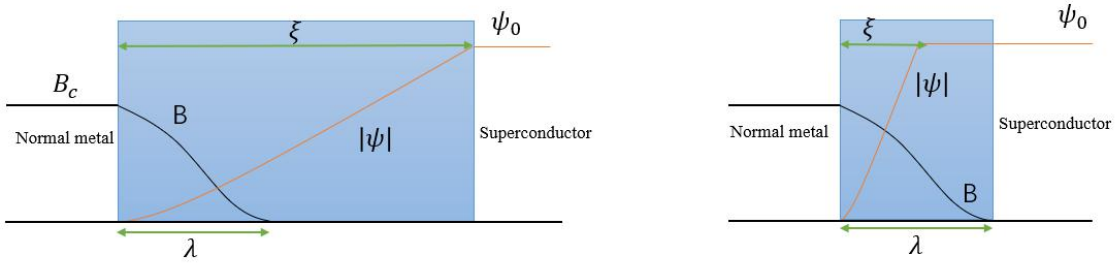

Figure 2.1: Sketch to understand Type I superconductor (left) and Type II superconductor (right). The radio of penetration depth λ and coherence length ξ will decide whether it is Type I or Type II superconductor.

Here we listed several common superconductors' coherence length and penetration depth [44]:

Table 2.1

Material	Coherence length ξ(nm)	Penetration depth λ_L(nm)	Ratio λ_L/ξ
Sn	230	34	0.16
Al	1600	16	0.010
Pb	83	37	0.45
Cd	760	110	0.14
Nb	38	39	1.02

From the table we can see Sn, Al, Pb, Cd are Type I while Nb is Type II.

BCS theory

The Bardeen-Cooper-Schrieffer (BCS) [38] model of superconductivity was built in 1957. At sufficiently low temperatures, electrons near the Fermi surface become unstable against the formation of Cooper pairs. Cooper showed such binding will occur in the presence of an attractive potential. In conventional superconductors, an attraction is generally attributed to an electron-lattice interaction. The BCS theory, however, requires only that the potential be attractive, regardless of its origin. In the BCS framework, superconductivity is a macroscopic effect which results from the condensation of Cooper pairs.

BCS theory predicts the dependence of the value of the energy gap Δ at temperature T on the critical temperature Tc. The ratio between the value of the energy gap at zero temperature and the value of the superconducting transition temperature (expressed in energy units) takes the universal value:

$$\Delta(T=0) = 1.764 k_B T_c \tag{2.9}$$

independent of material.

In superconductivity, the superconducting coherence length ξ is the characteristic exponent of the variations of the density of superconducting component. In some special limiting cases, for example in the weak-coupling BCS theory of isotropic s-wave superconductor it is related to characteristic Cooper pair size:

$$\xi_{BCS} = \frac{\hbar v_F}{\pi \Delta} \tag{2.10}$$

Where v_F is Fermi velocity, which is related with Fermi energy. In a general sense, it will be still reasonable for estimate the coherence length. Therefore, we can see the coherence length is closely connected with Fermi velocity.

Note that ξ_{BCS} is different from ξ in the GL theory.

2.2 Semiconductor properties of nanowires

In this section, I would like to introduce the field-effect transistor (FET)[39], which was demonstrate in 1960s. The metal-oxide-semiconductor FET (MOSFET), one of the classes of FETs, has made great contribution to the digital information technology. We will then discuss the silicon nanowire field effect transistor, which is the key object during our experiment. Furthermore, we would like to introduce quantization of conductance.

Figure 2.2 shows the cross section of the n-channel MOSFET. The source and drain terminals are separated by the p-type substrate with zero bias ($V_{GS} = 0$). However, if a large positive gate voltage which is greater than certain threshold voltage) is applied, an electron inversion layer due to the equilibrium band bending at the oxide-semiconductor interface is created. Electrons can thus move from the source into this region, and generate a current I_{DS}. This drain current could be expressed as:

$$I_{DS} = uC_{ox}\frac{W}{L}[(V_{GS} - V_T)V_{DS} - \frac{1}{2}V_{DS}^2] \tag{2.11}$$

Where u is the electron mobility, C_{ox} is the dielectric capacitance, $\frac{W}{L}$ is the radio between width and length of the channel, V_T is the threshold voltage, V_{GS} is the gate to source voltage, and V_{DS} is the drain to source voltage.

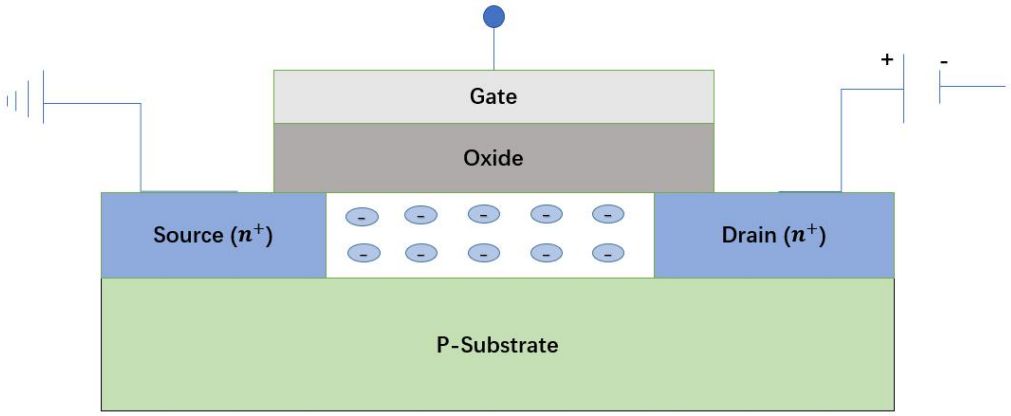

Figure 2.2: Cross section view of an n-channel MOSFET

When we put our semiconductor nanowire materials on this Si chip, it would perform like an field effect transistor (FET) as Figure 2.2 during electron transport measurement. The theory of MOSFET could be used as the reference and background for it. The Fermi level of materials would be tuned with a external electrical field by applying a voltage. We call it a "gate voltage (V_G)". In our experiments, we often use back gate voltage to tune these materials. The Si substrate is used as a gate contact and the thermal oxide is utilized as the gate dielectric.

The device structures were also developed from 3D bulk to the gate-all-around nanowire. The p substrate in n- channel MOSFET is then replaced by the intrinsic semiconductor nanowire. Again due to the band bending and thus the difference in the Fermi levels, electrons could move from the gate electrode to the nanowire.

See Figure 2.4. Below some voltage, the valence band would cross the Fermi level so that the carriers in the system depend on holes mainly, while above some threshold voltage (V_{th}), the conduction band would cross the Fermi level, and then carriers would depend on election in this case. These flow of electron carriers results in increasing conductance with the increasing gate voltage. It seems to open a channel between two electrodes inside semiconductor, which

is called pinch off. And the hole carriers have slight influence on the system so we always pay attention to the electron carriers of nanowires. Take InSb nanowire as an example. Figure 2.5 shows the conductance of InSb depending on the back gate voltage. In the beginning, the conductance of materials would remain almost zero. It is reasonable because semiconductor has such small conductance. Then the conductance would rise suddenly at some point (V_g), and reach to a highest voltage which called saturation region. For our InSb nanowire materials, we find it could reach to saturation region at 9 G_0 ($\frac{2e^2}{h}$). Additionally,we use hybrid semiconductor-superconductor materials compared to bare semiconductor. Therefore, the high conduction level of metal would lead to high conductance below V_{th} instead of just almost zero conductance.

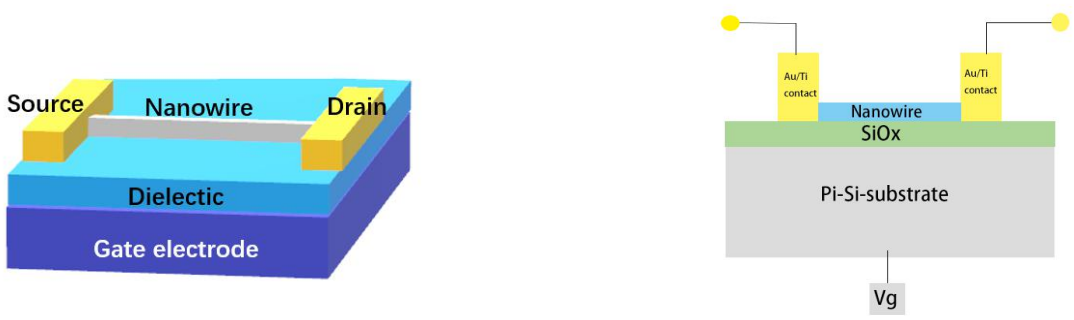

a b

Figure 2.3: Semiconductor nanowire on the SiOx substrate. It would behave as a field effect transistor (FET). **a)** is the schematic diagram of a single nanowire field effect transistor. **b)** is the cross section view of NW-FET

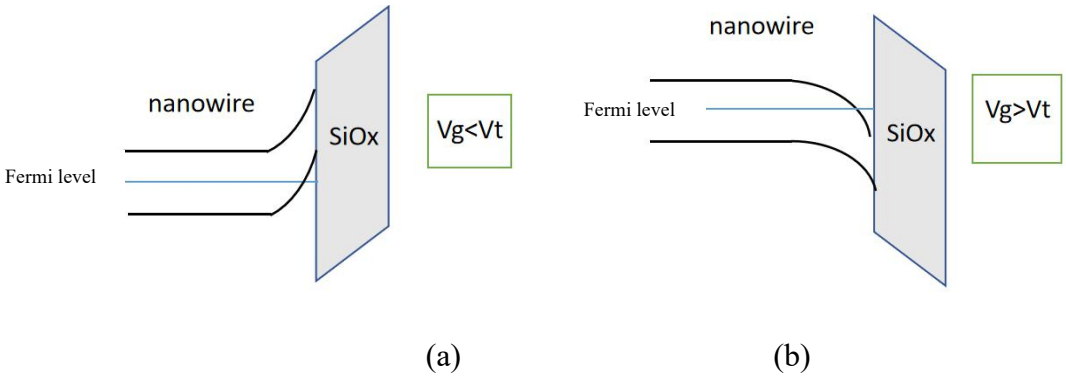

Figure 2.4: Band structure of semiconductor NW-FET. When we apply the gate voltage to the SiOx substrate, the Fermi level of nanowire on this substrate would be tuned.

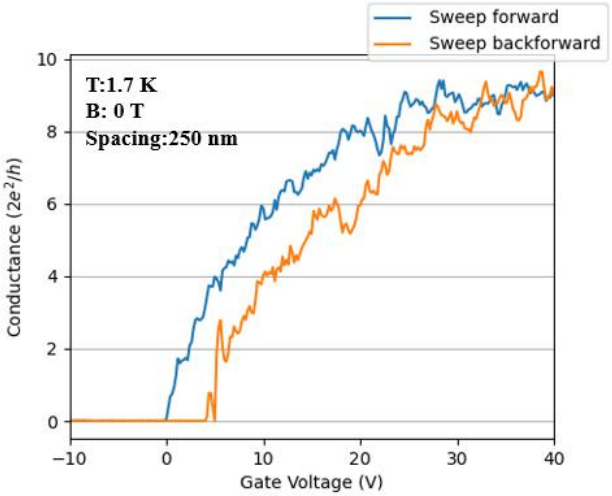

Figure 2.5: Example of pinch off curves of an InSb nanowire device (four probe method). At some threshold voltage (V_{th}), it would open a channel for electron carriers, and an increasing conductance could be observed clearly until it reaches saturation region. Below this threshold voltage, we could also see the conductance increases with the decreasing voltage. It makes little contribution to the conductance so we would not focus on it.

Since we are studying nanowires during our experiment, which the diameter of the devices are comparable to the mean free path of electron. We are expecting ballistic/semi-ballistic transport in these nanowire devices, and what's more, the quantization of conductance [40].

Typically, the conductivity is written as $\mathrm{G} = \frac{\mathrm{I}}{\mathrm{V}}$, and what we should concern with is the quantization of current. $\mathrm{I} = \frac{\mathrm{nev}}{\mathrm{L}}$, where n is the number of electrons in the direction of propagation, v is the electron velocity, and L is the length over which the motion takes place. By considering the density of state

$$dN(\mathrm{k_z}) = \frac{\mathrm{dk_z}}{\frac{2\pi}{\mathrm{L_z}}} = 2\frac{L_z}{h}\frac{1}{v_z}dE \tag{2.12}$$

We could obtain a differential equation

$$\frac{dN}{dE} = 2\frac{L_z}{h}\frac{1}{v_z} \tag{2.13}$$

Therefore, the number of electrons we mentioned above could be described as

$$\mathrm{n} = \sum \frac{2L_z}{hv_z}\mathrm{eV} \tag{2.14}$$

Return to the expression of current, it could be rewritten as

$$\mathrm{I} = \sum \frac{\mathrm{e}v_z}{\mathrm{L_z}}\frac{2\mathrm{L_z}}{hv_z}\mathrm{eV} = \frac{2\mathrm{e}^2}{\mathrm{h}}\sum 1 \tag{2.15}$$

where $\sum$ is the summation of occupied modes in the k_z transmission direction. We could write it as an integer number M. Now the conductance is expressed as

$$\mathrm{G} = \frac{2\mathrm{e}^2}{\mathrm{h}}\mathrm{M} \tag{2.16}$$

This equation shows the quantization of conductance. In the experiments, we may observe the conductance showing several plateaus with the increasing of gate voltage. Like Figure 2.6, it is a bare InSb nanowire measured at 1.7K, and it could show the quantized conductance at high magnetic field.

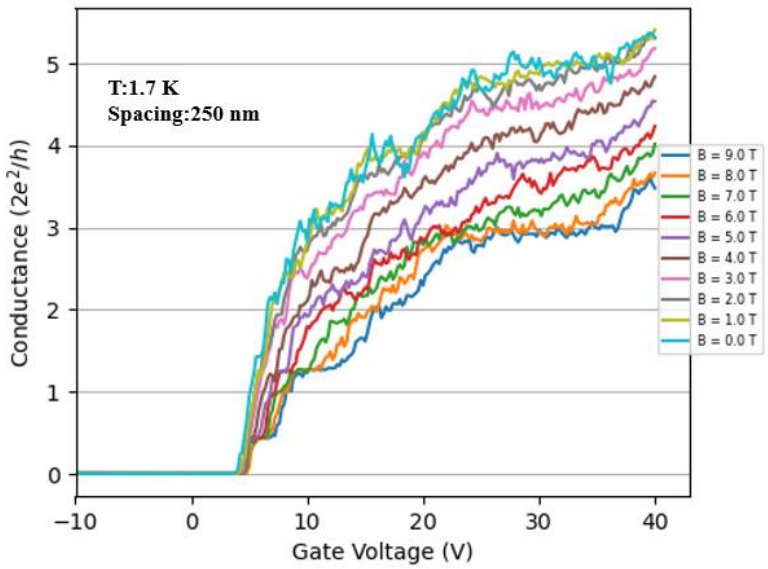

Figure 2.6: Example of an InSb nanowire device that shows conductance of quantization (two probe method). With the increasing gate voltage and magnetic field, the conductance shows several plateaus.

Chapter 3 Sample preparation and experimental setups

In this chapter, the process to get to nanowire devices for electronic characterization is introduced, from NW growth to device fabrication. Besides, we will also concern the measurement techniques and experimental setup. The growth work is completed by Yu Liu.

3.1 Growth

Vertical NWs:

Stem-assistant InSb(As) NWs were grown on 1/4 2-inch undoped n-type (111)B zinc-blende InAs wafers (Semiconductor Wafer Inc.) with the VLS method in III-V growth chamber of a solid-source Varian GEN-II MBE system with the background pressure below 1E−10 Torr [41]. The natural oxidized layers were desorbed from the InAs by heating the substrate to a temperature of 540 °C (measured with a pyrometer) under As2 overpressure protection for 360 s. To get the right density and diameter of NWs, the Au beam (deposition rate of 9E−4 nm/s) that form the Au catalysts was open for only 3 sec, giving a NW density around 0.044 /μm2. InAs stems were grown with As4 at a substrate temperature of 447 °C (measured with a thermo-coupling back sensor) for 720 s. The corresponding planar growth rate was 0.32 μm/hr and the As4/In ratio of 10. After stem growth, InSb(As) NWs started to grow immediately after InAs stems were ready. The InSb(As) growth temperature was 447 °C (measured with a thermo-coupling back sensor) and the growth took 2400 s. The corresponding planar growth rate was 0.32 μm/hr and the Sb2/In ratio was 3.6 and the As4/In ratio was 0.4.

The substrates with as-grown InSb NWs were transferred from the III-V growth chamber to the metallic chamber right after growth. The substrates were cooling for 6 hours before deposition. The substrates had about 45° tilt towards the Pb source. Nominal 20 nm Pb layer

was deposited on two side facets of NWs with in-situ electron beam evaporation with a substrate temperature of -144 °C (measured with a thermo-coupling back sensor) and an average growth rate of 1.6 nm/s. A 2 nm Al layer was deposited with a growth rate of 0.06 nm/s on the Pb layer to stop it from dewetting during sample uploading. Pure oxygen of 10 Torr was used to oxidize the NWs in-situ for 10 s and thus the Al layer would become AlOx to protect the Pb layers on NWs side facets. After in-situ oxidization, the load lock was vented to 500 Torr with N2 to warm up the samples. It usually needed 5 min. After that, the samples would be unloaded.

Growth of NWs with shadow junctions

The NWs grown in trenches use (100) InAs wafers as substrates instead of (111)B InAs. The growth recipe for InSb(As) core is similar to that of vertical NWs. The difference is that the As4/In ratio was 0.9 for the NWs grown in trenches. The tilt angle was 27° towards the Pb source, which was supposed to deposit Pb on two side-facets of NWs.

The big difference in terms of method between vertical NWs and NWs with shadow junctions is that NWs with shadow junctions require additional substrate fabrication. The substrates are usually prepared in the following way:

1. Open trenches:
    a) Coat resist:
        i. Spin electron-sensitive copolymer resist EL9 with 4000 rpm (thickness ~ 320 nm) for 45 s.
        ii. Hot-plate bake the resist at 185 °C for 2 min to get rid of the solvent and improve the adhesion with the substrate.
    b) Expose design for the trenches with EBL.
    c) Develop:

i. 1:3 MIBK/IPA for 45 s.

ii. IPA for 30 s.

iii. N2 blow dry.

iv. Oxygen plasma ash for 2 min.

v. Hot-plate bake at 115 °C for 1 min.

d) Etch: Wet-etching is used to create V-shaped (111)B faceted trenches.

i. Mix H_2SO_4 (1 mL)/H_2O_2 (8 mL)/H_2O (80 mL) and blend it for 5 min with a magnetic stirrer.

ii. Take 4 mL of the above mixture, mix with 400 mL of H_2O, and blend it for 5 min with a magnetic stirrer.

iii. Dip the wafer into the solution for 36 min. The etch rate is ~ 2 μm/h.

e) Clean:

i. acetone for 4 min.

ii. sonication for 2 min with 80 Hz frequency and 30 W power.

iii. acetone for 10 s.

iv. IPA for 10 s.

v. Milli-q water for 20 s.

vi. Another Milli-q water for 2 min.

vii. N2 blow dry.

2. Place Au dots:

a) Coat resist: Two layers of resist are needed to coat homogeneously on the wafer with trenches.

i. Spin EL6 with 4000 rpm (~ 150 nm) for 45 s

ii. Bake at 185 °C for 1 min.

iii. Spin A2 with 4000 rpm (~ 60 nm) for 45 s

iv. Bake at 185 °C for 1 min.

b) Expose design for the Au dots with EBL.

c) Develop:

i. 1:3 MIBK/IPA for 45 s

ii. IPA for 30 s

iii. N2 blow dry.

iv. Confirm that the dots are properly aligned with the trenches with the optical microscopy.

d) Deposit Au at the rate of 1 Å/s using an e-beam evaporator. The thickness of Au layer is 12 nm. Note: If there is a time delay between resist development and Au deposition, it is crucial to remove the native oxide of InAs before Au deposition by hydrofluoric acid (HF) dipping or in-situ Ar milling in the evaporation chamber.

e) Lift-off

i. Heat water in the water bath to 50 °C

ii. Acetone, which is placed into the 50 °C water bath for 30 min

iii. Blow the wafer in the acetone with a plastic dropper

f) Clean:

i. acetone for 10 s.

ii. IPA for 10 s.

iii. Milli-q water for 20 s.

iv. Another Milli-q water for 2 min.

v. N2 blow dry.

vi. Oxygen plasma ash for 2 min.

g) Cleave the 2 inch wafer into four quarters.

Figure 3.1: The photo of the MBE system for sample preparation. The III-V growth chamber is marked with "III-V" and the metallic chamber is marked with "Metallic".

Structural Characterization

The morphology of NWs together with substrates was characterized by scanning electron microscope (SEM) in JEOL 7800F. The JEOL 7800F is a 30 kV field emission SEM equipped with two secondary electron detectors and it has an eucentric stage. The microscope is shown in Figure 3.2.

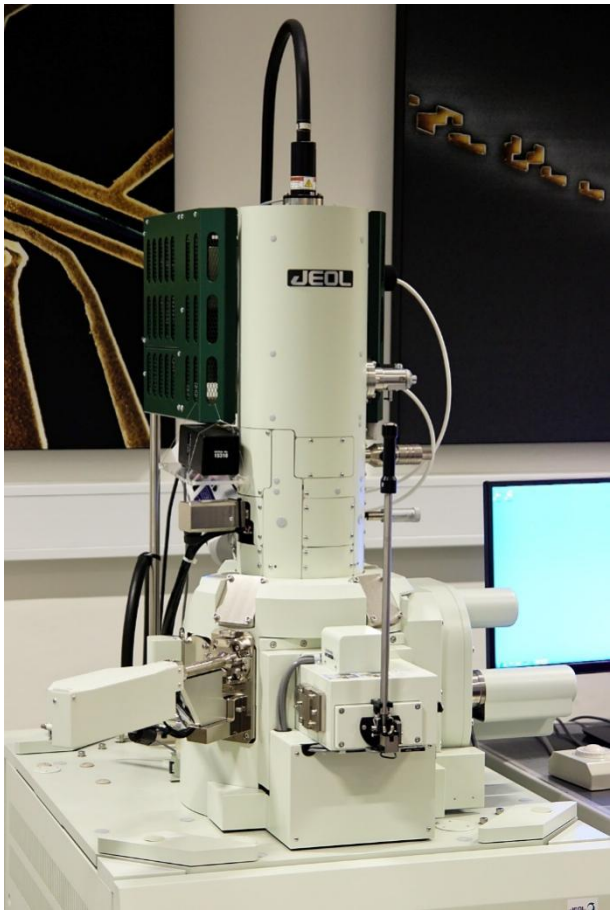

Figure 3.2: The photo of JEOL 7800F SEM.

Both a FEI Versa 3D and a Tescan GAIA focus ion beam – scanning electron microscope (FIB-SEM) were used for TEM cross-section sample preparation. Both FIB-SEMs are equipped with Omniprobe micromanipulators for lifting out TEM lamellas. Both instruments can go down to ~ 1 kV in ion beam energy for gentle milling of the TEM sample in the final stage. Those set ups are important for preparing high quality TEM samples from nanowires.

A JEOL monochromated NEO ARM was used for transmission electron microscopy (TEM) study. The microscope is equipped with a double Wien-type monochromator, probe Cs corrector and image Cs corrector, as well as STEM ADF, BF detectors. The microscope is also equipped with a Continuum Gatan Image Filter (GIF) with direct detection camera. The high tension of the TEM can be varied between 40 and 200 kV. Probe Cs corrector is essential for directly imaging the structure details at the interface between the superconductor

and semiconductor at the atomic scale. Monochromator and GIF Continuum will enable high energy resolution (< 30 meV) electron energy loss spectroscopy (EELS) study of chemical composition and electronic structure at the interface. The possibility of going to relatively low high-tensions can reduce beam damage during TEM analysis.

A FEI Titan microscope equipped with a Wien-type monochromator, a probe Cs corrector and a GIF Tridium EELS spectrometer was used for TEM investigations. The probe Cs corrector will enable atomic resolution high-angle annular dark-field (HAADF) aberration corrected scanning transmission electron microscope (AC-STEM) image imaging, while monochromator and EELS spectrometer will allow high resolution (~ 0.1 eV) EELS analysis of the interface.

There was no evidence to show that Pb layers could grow on InSb specific facets. The as-grown InSb/Pb NWs are shown using SEM. It can be seen that there is thickness variation of the Pb layer along NWs. With low-resolution TEM, the Pb layer is estimated to be 30 nm. The AlOx layer with a thickness of 2-5 nm can also be observed in the TEM image. To understand the lattice match between InSb and Pb, we did atomic resolution TEM imaging on the InSb/Pb NWs. We started with checking the interface between InSb and Pb in the transverse view. We can see the single crystalline zinc-blende InSb lattice without mislocation or misplacement. However, there are no lattice fringes in Pb area when the zone axis is along InSb [1-10]. We then rotated the NW and orientated the Pb layer to align that zone axis with the electron beam. The image suggests that the Pb layer is free of defects and impurity. However, the Pb [1-10] zone axis is tilted at least ~10° with respect to the InSb [1-10] zone axis, so the Pb layer is not epitaxial on InSb side facets. It is different from InSb/Al, but it could have positive influence. On one hand, the InSb/Pb interface could weaken the potential proximity effect. On the other hand, there will be no stress due to lattice mismatch.

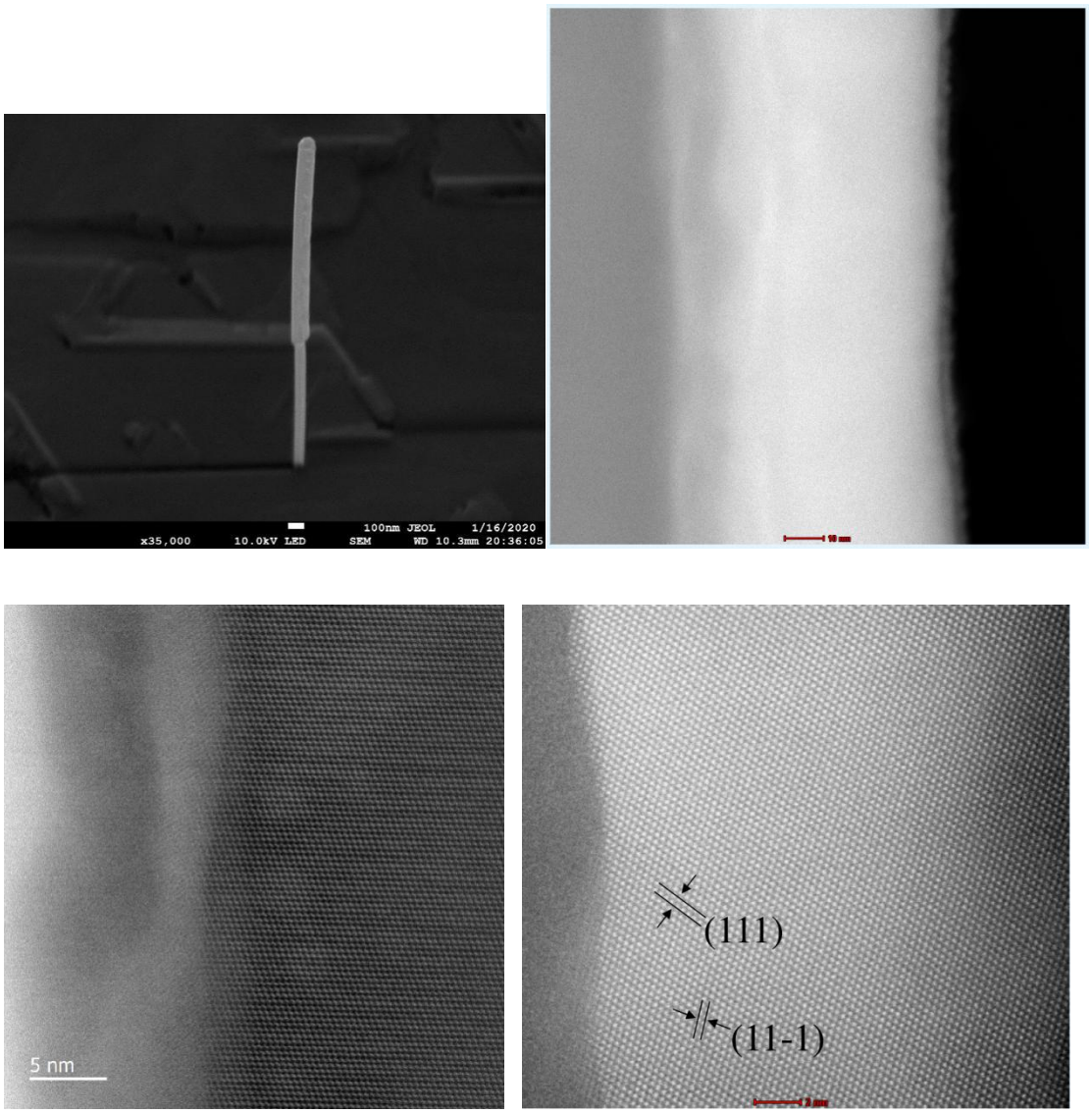

Figure 3.3: TEM image of InSb/Pb. This work is done by LunJie Zeng at Chalmers. The transmission electron microscope used in this work is an FEI Titan 80-300 microscope equipped with a Schottky field emission gun, a monochromator and a probe Cs corrector. The microscope was operated at 300 kV for imaging and diffraction. Scanning TEM (STEM) was performed with a beam semi-convergence angle of ~ 20 mrad and a semi-collection angle from ~ 54 mrad to ~ 270 mrad.

To explore the lattice match between InSb and Pb, we employed Kikuchi pattern analysis in transmission electron microscope. Kikuchi lines are patterns of electrons formed by inelastic

scattering followed by Bragg scattering of the incident electrons. The lines pair up to form bands in electron diffraction patterns from single crystal specimens, there to serve as "roads in orientation-space" for microscopists. In transmission electron microscopes, they are easily seen in diffraction from regions of the specimen thick enough for multiple scattering. Unlike diffraction spots, which blink on and off as one tilts the crystal, Kikuchi bands mark orientation space with well-defined intersections (called zones or poles) as well as paths connecting one intersection to the next.

Figure 3.4: The photo of FEI TITAN microscope

3.2 Device Fabrication

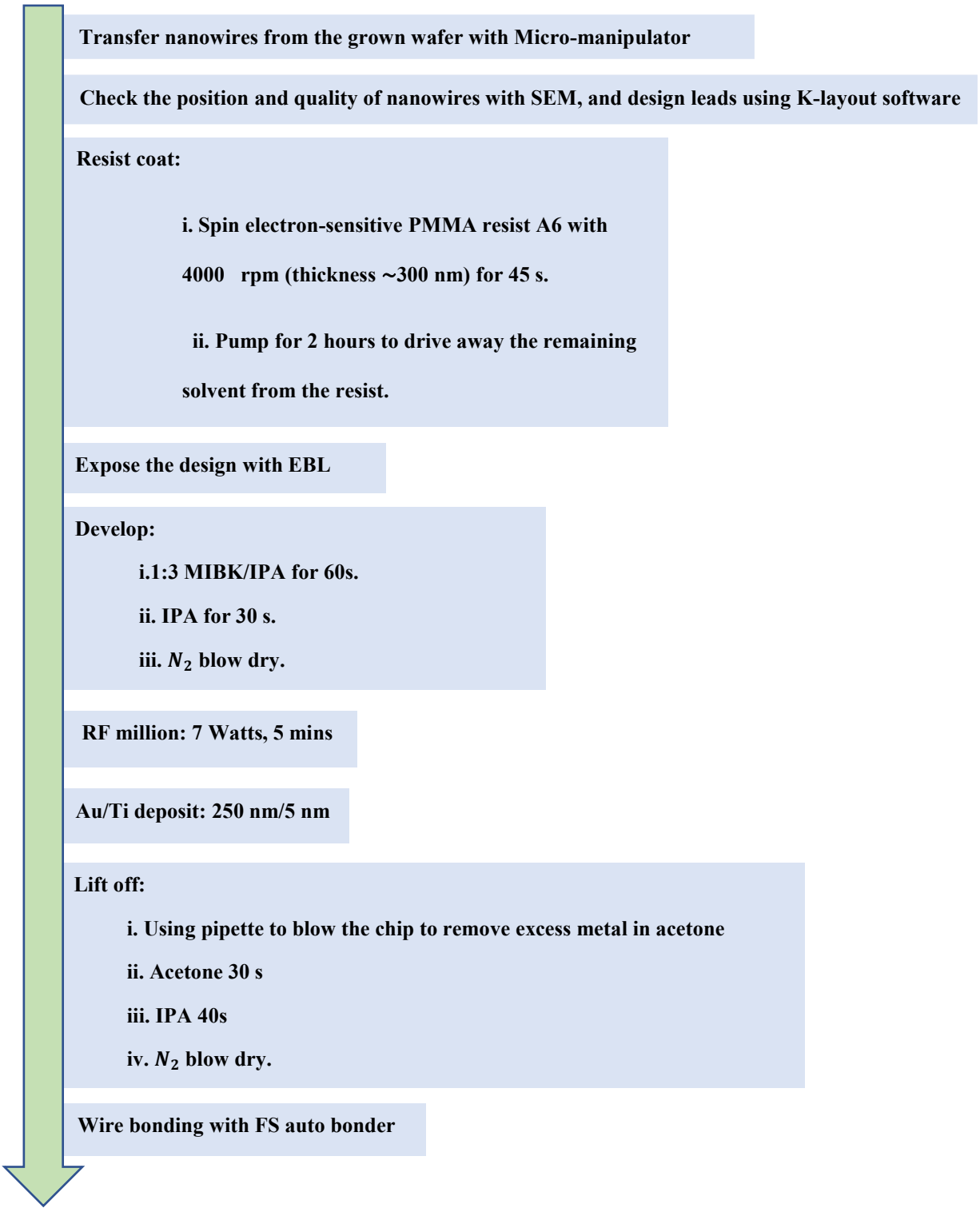

Figure 3.5: Flow-process diagram for InSb/Pb and InAsSb/Pb devices fabrication.

In this section, the process and tools for two-probe/four-probe device fabrication with the goal of electronic transport measurement will be presented. The fabrication process for all devices of both InSb/Pb and InAsSb/Pb NWs in this project is similar. The overview of our fabrication process is shown in Figure 3.5, and the experiment setups used during fabrication will be introduced afterwards.

Note for process:

In the beginning, when I were using plasma asher to clean the chip after I had deposited Au leads on the nanowires according to the former recipes our group ever used, I found Pb would be greatly destroyed. It is speculated that the heat from plasma ash can be conducted via the Au leads. Because the residual resist will have minor effect on measurements, we decide to remove this step.

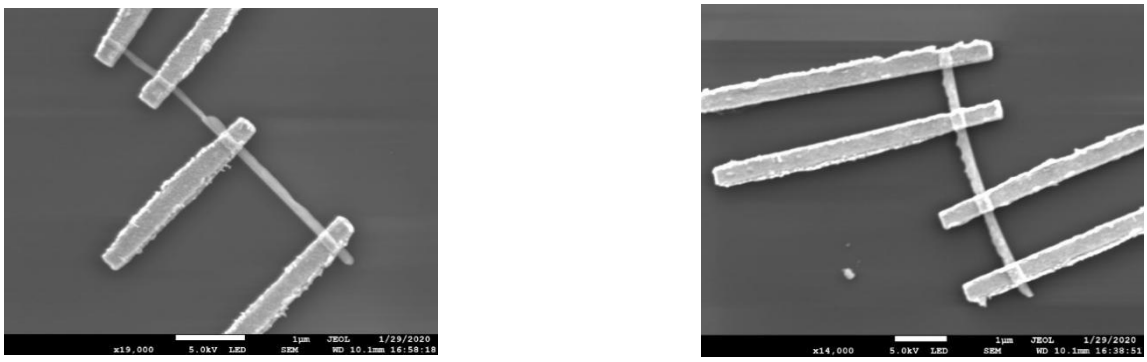

Figure 3.6: Left panel: four-probe device of InSb/Pb nanowire; Right panel: Four-probe device of InAsSb/Pb. Pb is destroyed compared with Figure 3.7.

Micromanipulator. It is a tool that can transfer nanowires from a sample substrate to a chip. It consists of an joystick and a stage for the movement of the needle with minimum step of 0.1 mm. We can attach the needle to a nanowire by Van der Waals force and then transfer the nanowire on a chip with Si-SiO2 substrate. The advantage of the method is selectivity, because we could deposit the nanowires both with and without shadow junctions on the same chip.

Scanning electron microscopy (SEM). It is a microscope that uses a focused electron beam scanning over a surface for imaging, which has been shown in Figure 3.2. The images from SEM can reach the resolution of better than 1 nanometer, and therefore, we are able to investigate the position and the quality of Pb layers on the facets of nanowires and choose the nanowires for device fabrication. After SEM imaging, I would design the metallic leads with software Klayout according to the images.

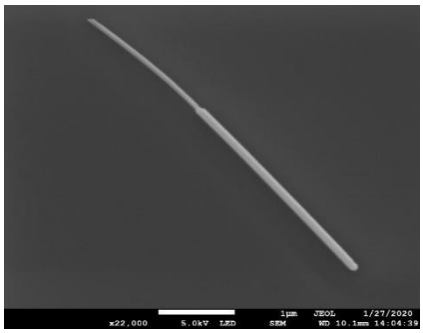

(a) InSb/Pb nanowire

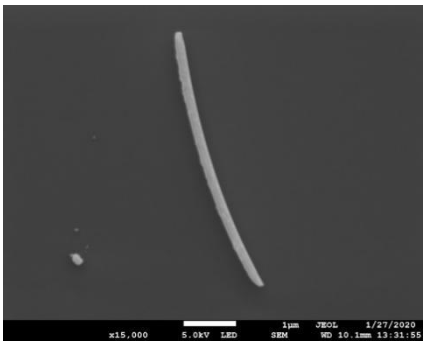

(c) InAsSb/Pb nanowire

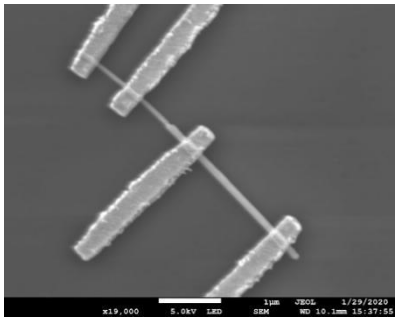

(b) After Ti/Au deposition

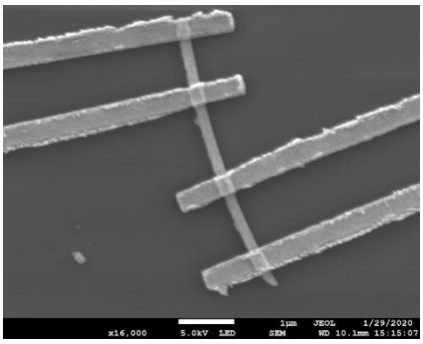

(d) After Ti/Au deposition

Figure 3.7: SEM images of InSb/Pb and InAsSb/Pb (a), (b) are InSb/Pb in the process. (c),(d) are InAsSb/Pb in the process.

Electron beam lithography (EBL) EBL consists of spin coating, exposure and development steps. EBL uses electron beam resist, a kind of polymer, of which the focused electron beam can break the covalent bonds. The exposure feature sizes would down to 10

nm. However, during exposure, the electron beam will widen due to electron scattering in the resist and substrate material. Therefore, the patterns and corresponding dose time need to be corrected. Here, we use a program called Beamer. After spin resist coating and pumping, I put the samples into the EBL. In this case, I would use Elionix100 with an electron acceleration voltage of 100 keV. Then, I developed the sample with MIBK:IPA (1:3) solvent.

AJA deposition system. AJA is a thin film deposition system including ion milling and e-beam evaporation. For ion milling, Ar ions generated by the RF signal hit the negatively charged stage inside the vacuum chamber, so they will remove the oxide layer on the surface of samples. The e-beam evaporation system would offer a variety of deposition sources. In this case, I used Ti and Au for making leads.

FS autobonder

To conduct electronic measurement, we need to contact wires between devices on a chip and a daughterboard. Here we use FS autobonder to do wire bonding. The chip will at first be attached on the daughterboard with silver paint. The silver paint is conductive, so it is possible to have an electrostatic back gate for the chips during the measurements. Then, we bonded leads and pads (15 diam of bond force, 70 digits of US power, and 35 ms of total bond time) for two- or four-probe devices. One more pad is bonded with the inner surface of daughterboard to build a back gate. The bonding is conducted according to a bonding scheme .

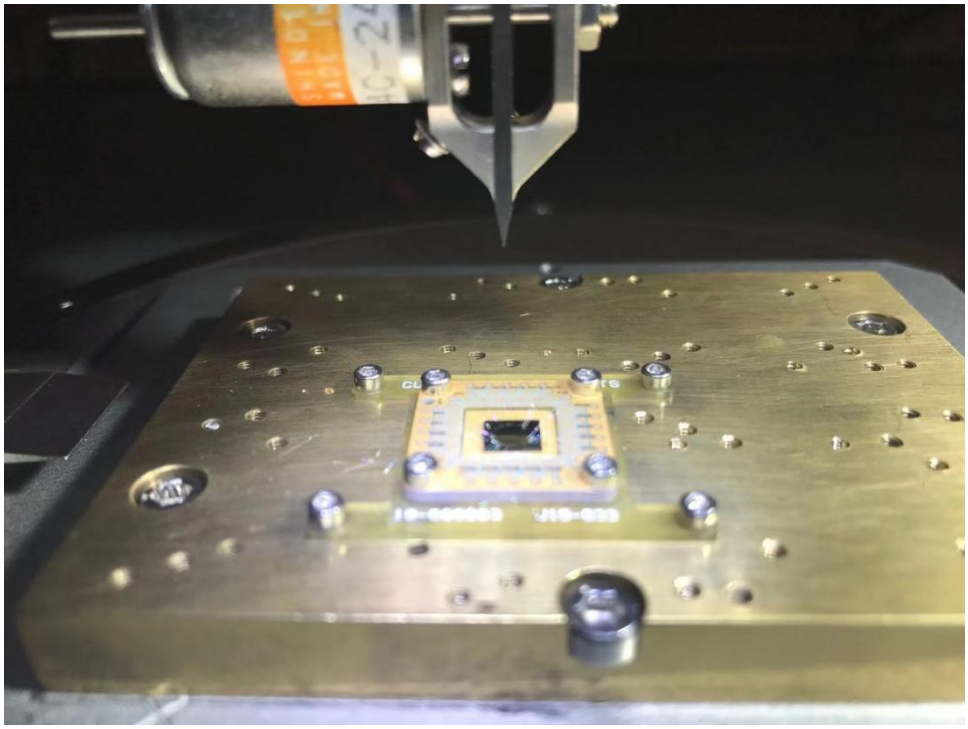

Figure 3.8. Image of a loaded chip during bonding. Each lead of devices on the chip is contacted with one pad on a daughter board.

3.3 Measurement Setup

The system for electronic characterization we use is a Dynacool cryo-cooled physical property measurement system (PPMS) with temperature range of 1.7K – 400K, and perpendicular magnetic field from 9 T to -9 T.

The Dynacool PPMS:

The Dynacool PPMS contains three components: the cryostat, cryopump/magnet cabinet, and CAN module bay. The cryostat transfer Helium to the cryopump to control the flow and thus the temperature. The CAN module bay is an external controller attached to the cryostat to set the conditions for the measurement vis ethernet. The system makes use of a single, two-stage pulse tube cryocooler, providing a low environment and low maintenance costs for

measurements. Figure 3.10 shows the He gas circulation inside the PPMS, which consist of two plates at 45 K and 4.2 K. These two cooler stages, which enclosed in a chamber of helium gas, and liquid environment called “bucket”, are the key components to result in a low temperature. The bottom of this bucket is covered with liquid He, and is connected to the “4 K plate”, and this plate is in contact with the superconducting magnet directly. What’s more, to achieve a 1.7 K base temperature, there is cooling operation called “low-temperature flow”. When the temperature reaches below 10 K, a capillary from the bottom of bucket flows helium gas to the sample chamber. The difference of enthalpy on the two sides of the capillary and gas that pumps from the anulus drop the temperature below 4.2 K. This transfer leads to 1.7 K liquid/gas helium mixture.

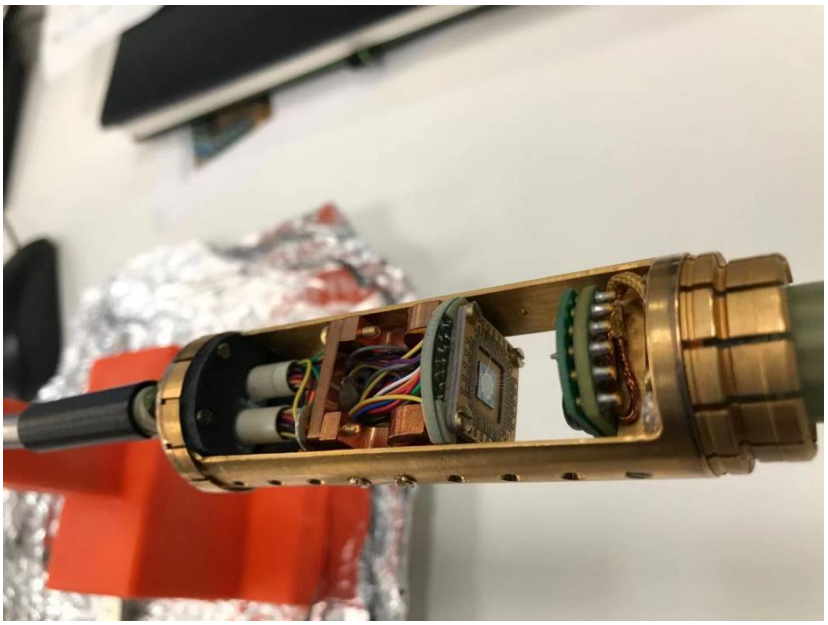

Figure 3.9: The sample in the motherboard waiting for loading in the PPMS

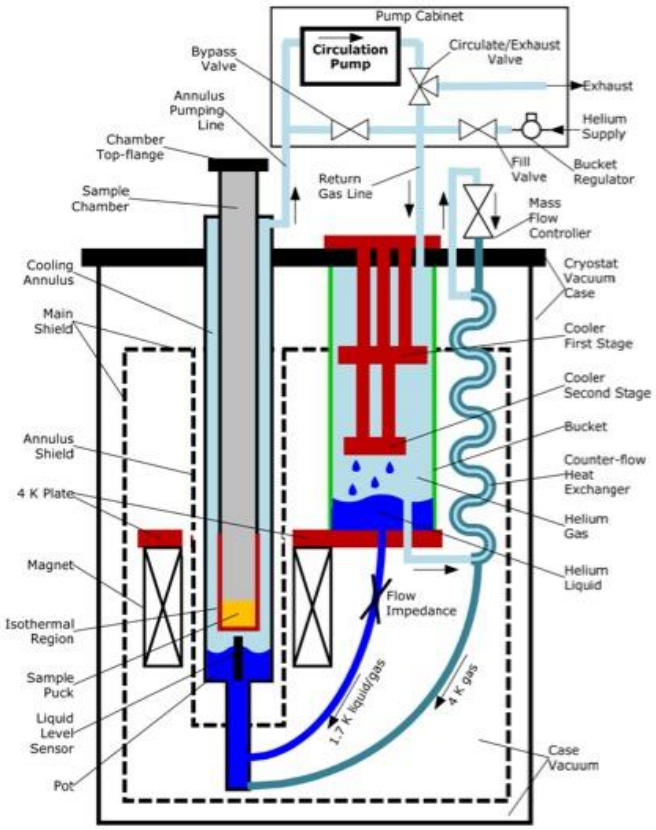

Figure 3.10: The dynacool PPMS. The schematic with the pumps, chamber and main PPMS system. It is taken in from Ref.[42]

Qcodes

Qcodes is a Python-based and an open source date acquisition framework for physics experiments controlled easily by computer with many degrees of freedom. It is developing by the collaboration with Station Q in Copenhagen, Delft, and Sydney. We use Qcodes for the measurement operation. All the operation including the change of temperature, magnetic field, and the gate voltage will be controlled by Qcodes.

Lock in amplifiers

All measurements are done with lock-in amplifiers (SR830) to measure the differential conductance. Lock in amplifiers are excellent measurement setups to detect very small AC

signals accurately even when there are many noise sources. The Schematic diagram of the measurement at low temperature is shown in the following.

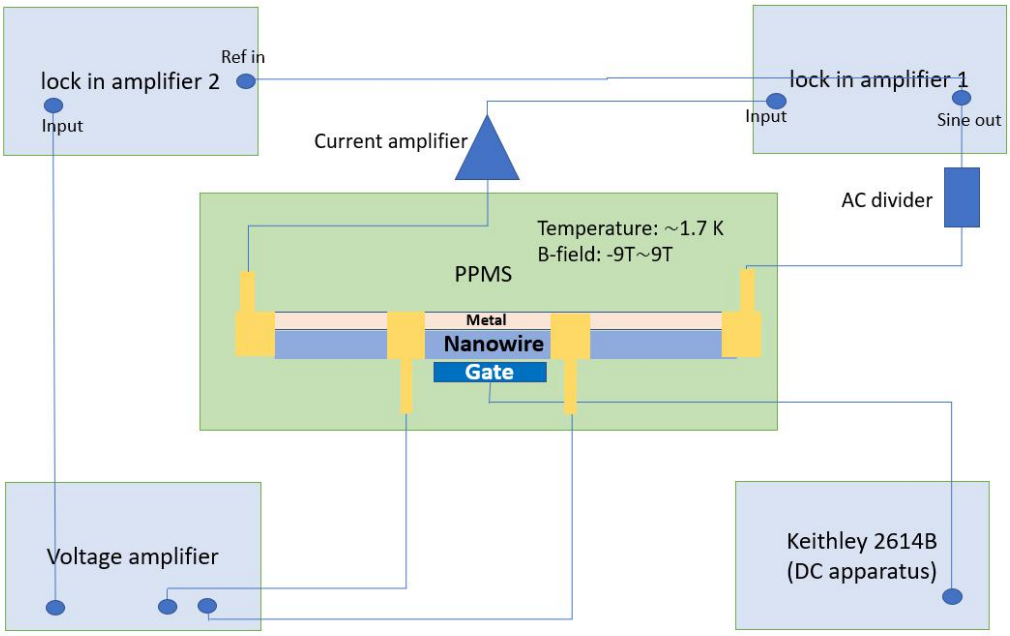

Figure 3.11: Schematic diagram of the experiment setup (Four probe measurements). The sinusoidal waveform voltage is applied by the lock in amplifier 1, and it is divided four orders of magnitude with an AC divider. This signal will go through the current amplifier and finally be read by the lock in amplifier 1 using the formula $I_{in} = KV_{out}$, where K is the gain from the current amplifier. The lock in amplifier 2 will read the voltage drop V_{drop} in the middle part. Then the difference conductance can be given by $G = \frac{I_{in}}{V_{drop}}$. The Keithley 2614B will apply an DC signal t to tune the Fermi level of the semiconductor nanowire as the gate voltage.

Chapter 4 Results and discussion

In this chapter I will present results of our electrical characterisation on Qdev999 InSb/Pb VLS nanowires (no shadow junction) and Qdev996 InAsSb/Pb VLS nanowires (with shadow junction). The standard lock-in technique is used to measure differential conductance by applying a small AC excitation voltage and then measuring the AC current I_{AC} and the voltage drop between channel of the device like Figure 3.11 above.

4.1 Qdev999 InSb/Pb VLS nanowire

The first low temperature measurements performed at PPMS we focus on was Qdev999 InSb/Pb VLS nanowire. We want to know whether it could show basic superconductor and semiconductor properties. The top-view SEM image of the device is shown in Figure 4.2b.

Most of current will go through a Pb layer if it is continuous along the NW without a junction. It also provides the opportunity to study the superconductivity of Pb and the potential influence of InSb/Pb interface and oxide surface, since the layer is thin. Here we would use four-probe devices. Temperature and field dependence of these devices were studied by swapping the magnetic field perpendicular to NW from -3 T to 3 T in the temperature range from 1.7 K to 9 K. Figure 4.1 shows the clear superconducting region. We found the resistance dropped down to zero ohm at around 7.0 K, similar to that of bulk Pb. Based on the relation described above (Equation 2.9), the BCS superconducting gap 2Δ of the Pb layer is almost the same as that of bulk Pb, which is 2.13meV. On the other hand, the critical temperature T_c decreased when the magnetic field H_c increased with a quadratic dependence relationship, which agrees with the the formula $H_c(T) = H_c(0)\left[1 - \left(\frac{T}{T_c}\right)^2\right]$. The critical temperature T_c became 1.7 K when the field was around 1.14 T. Then the critical field H_c is

estimated to be 1.27 T when T=0, which is much larger than 0.08 T of bulk Pb [43,44]. The fit to the data is shown in Figure 4.1c.

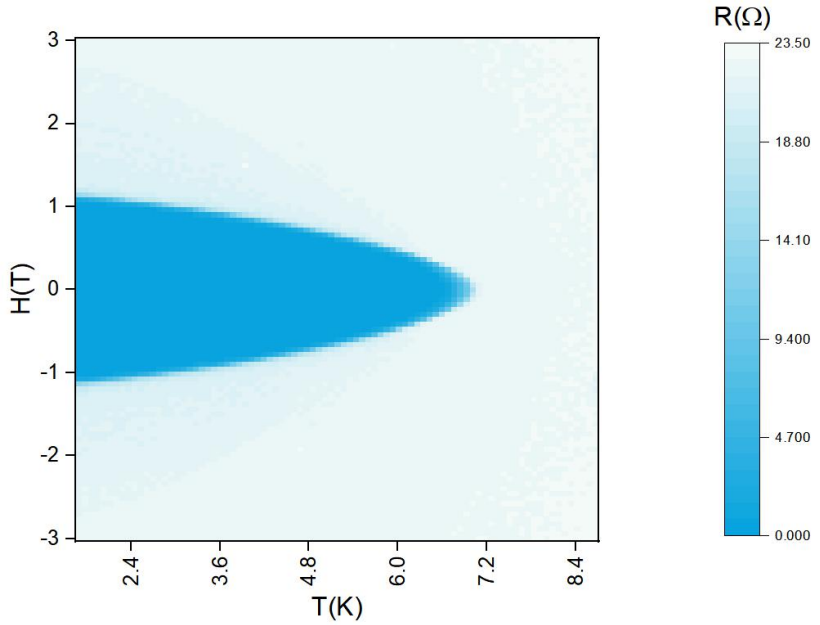

a

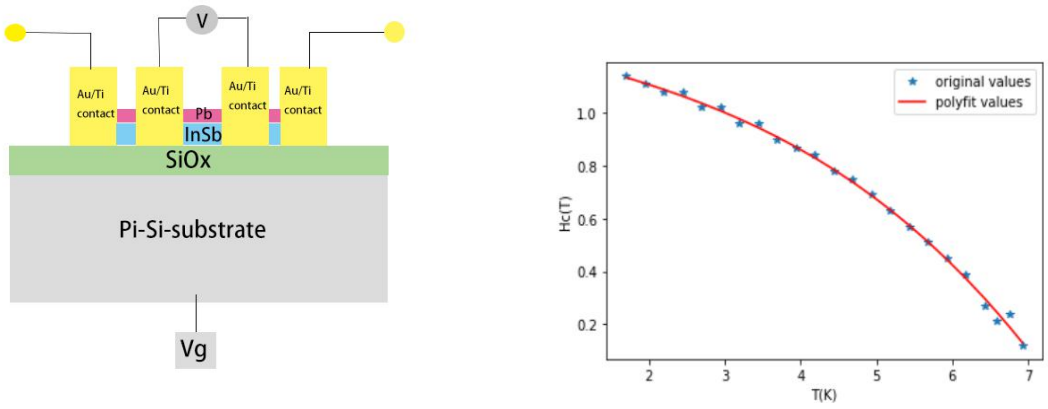

b **c**

Figure 4.1: a) The thermodynamic phase diagram for a InSb/Pb VLS nanowire with four probe method. Temperature sweeps from 1.7 K to 9 K, and magnetic field from -3 T to 3 T. **b) Schematic diagram of cross section view of InSb/Pb nanowire.** It is measured with four probe method. The voltage drop between the channel and the current that flowing through this device could be measured by standard lock-in technique,

leading to the conductance and resistance of the nanowire. **c) Critical field as a function of T.** The blue points are original experimental date, and the red curve corresponds to the fit to the data.

Having obtained the clear superconducting phase of Pb, we expect its reaction with the gate voltage result from the inherited properties of the InSb nanowire. To characterise this we continue to perform the field effect transistor measurements with the device geometry shown in Figure 4.1b. The Pb has thickness of 50 nm according to TEM measurement so that it would show very large conductance.

Figure 4.2 shows differential conductance, G with the back voltage with the range from -40V to 40V. We measured tons of devices with 4 probe setup. Most of them showed flat curve with gate voltage. The conductance usually has 800 G_0 to 1000 G_0, and we usually had hard time to obverse its gate tunability, but few of them could pinch off, see Figure 4.6. We obverse it at 7.5 K since it would change to superconducting region at low temperature.

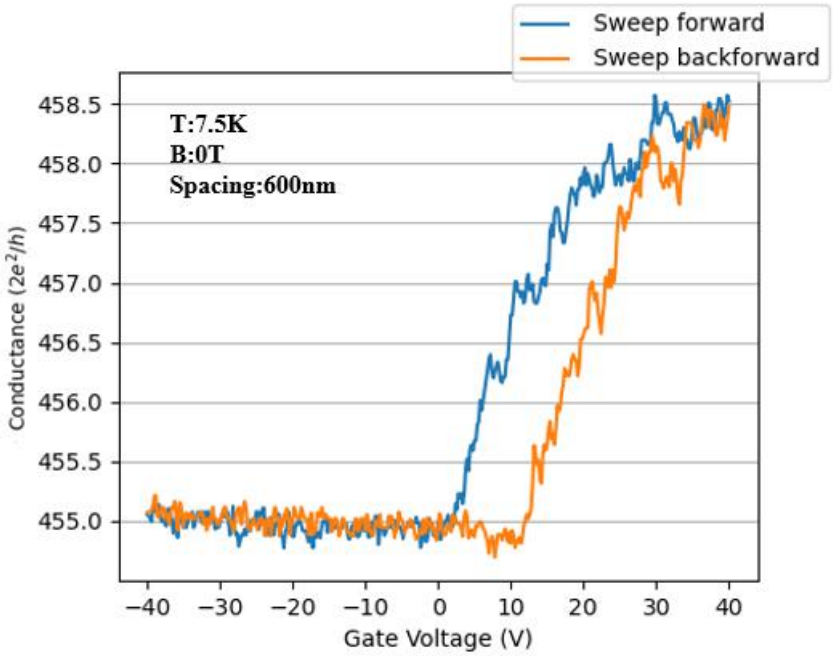

a

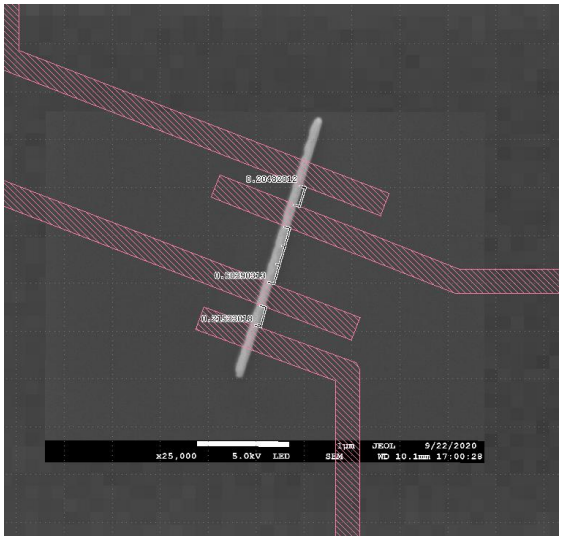

b

Figure 4.2: a) Pinch off curve of electron transport on InSb/Pb VLS nanowire. The blue line shows gate voltage sweep from -40 to 40 V, and the origin line shows gate voltage sweep from 40 to -40 V. **b) SEM image of InSb/Pb nanowire.** Four probe method was used. The spacing between contacts is 600 nm.

4.2 Qdev996 InAsSb/Pb VLS nanowire

In the following part, I would like to show results from the electron transport measurement on Qdev996 InAsSb/Pb shadow junction nanowires. The devices geometry given in Figure 4.3b and Figure 4.4c. Figure 4.4d shows a SEM image of one of the InAsSb/Pb shadow junction nanowires. We first chose nanowires that didn't contain the shadow parts to observe the superconductivity with four probe method. After two probe method for studying semiconductor properties of these shadow junction nanowires would be presented. Ballistic transport behavior are realized in one of these devices.

InAsSb/Pb also shows clear superconducting phase with critical temperature 7.1K and critical magnetic field 0.8 T, proving its successful Pb covering on the InAsSb. Shown in Figure 4.3a.

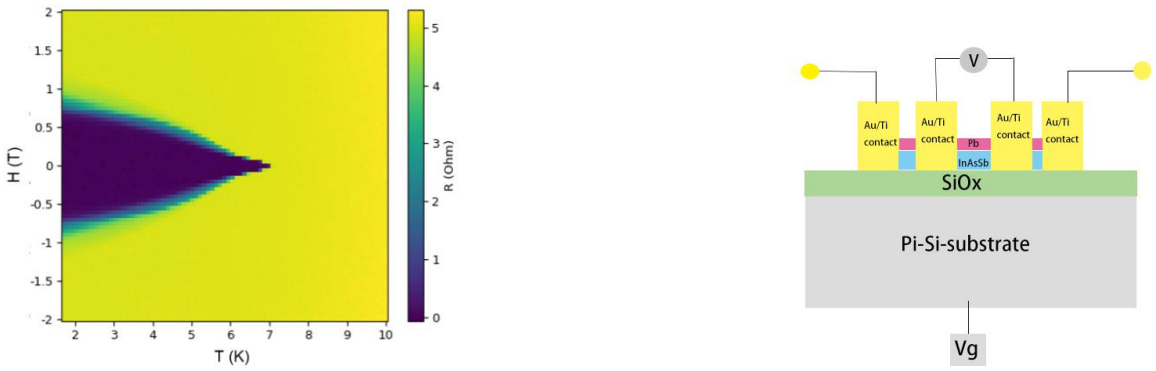

a **b**

Figure 4.3: a) The thermodynamic phase diagram for a InAsSb/Pb VLS nanowire. Temperature sweeps from 1.7 K to 10 K, and magnetic field from -2 T to 2 T. **b) Cross section view of InAsSb/Pb nanowire.** It is measured with four probe method for this 2D map.

Then we focus on the shadow junction properties. We sweep the magnetic field from 0 T to 8 T. No quantized conductance plateaus are observed at zero magnetic field. But as the field is increased (at around 5 T), we succeed in finding the conductance plateau. Backscattering of electrons is suppressed by the high magnetic field, and it becomes flatter and obvious at higher magnetic fields. For this device we plot the conductance G with gate sweep from -30 V to 30 V. The formation of this step-like region which is close to 0.5 G_0($G_0 = \frac{2e^2}{h}$) is visible (around 0.44 G_0 due to influence from the contact resistance), and possibly there is a development of plateau at $1G_0$ at low magnetic field although it is less pronounced. The plateau at zero or pretty low magnetic field is difficult to be observed is because of many scattering events induced by impurities or imperfections in the crystal lattice. Ideally, in the absence of magnetic field, the spectrum shows the two-spin degenerate sub-bands, and each of them below the Fermi level will result into a conductance of $G_0 = \frac{2e^2}{h}$. With the increasing magnetic field, the spin- degeneracy is lifted due to the Zeeman effect, and it contributes to

an energy spacing $\Delta E_{subband} = E_{1\uparrow} - E_{1\downarrow} = g\mu_B B$. As a result, the quanzited conductance will give $\frac{e^2}{h}$ instead of $\frac{2e^2}{h}$ [46], as the Figure 4.4 shows.

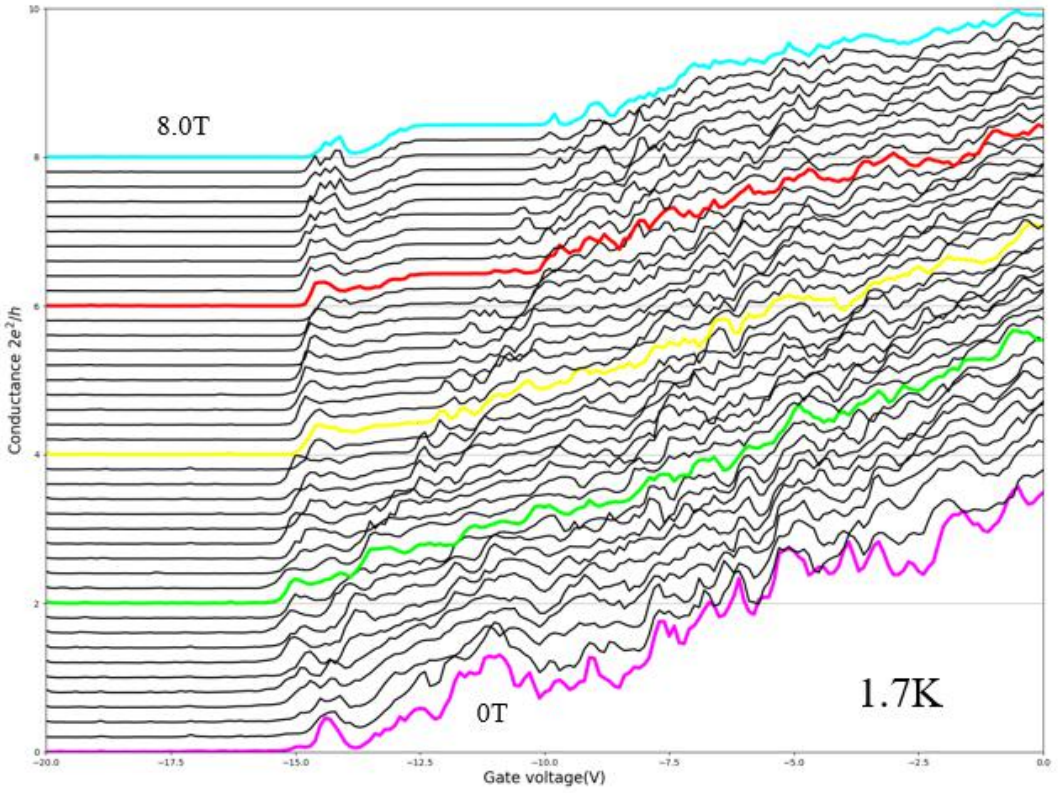

a

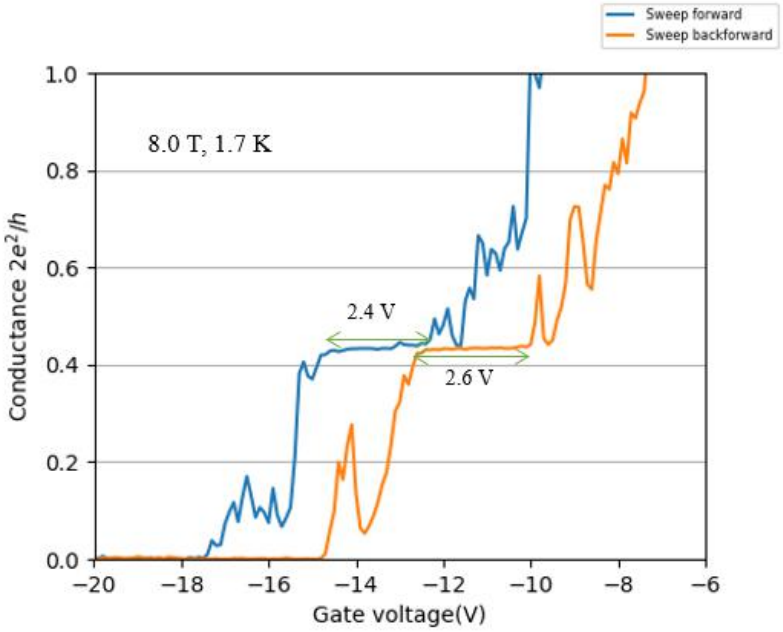
Sweep forward
Sweep backforward
8.0 T, 1.7 K
2.4 V
2.6 V
Conductance 2e²/h
Gate voltage(V)
1.0
0.8
0.6
0.4
0.2
0.0
−20
−18
−16
−14
−12
−10
−8
−6

b

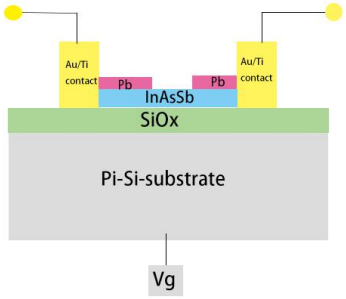
Au/Ti contact
Pb
Pb
Au/Ti contact
InAsSb
SiOx
Pi-Si-substrate
Vg

c

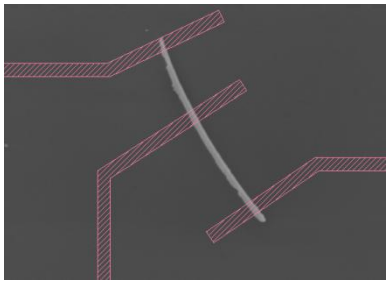

d

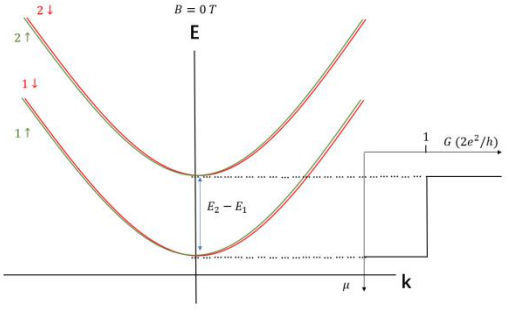
B = 0 T
E
2↓
2↑
1↓
1↑
1
G (2e²/h)
E₂ − E₁
μ
k

e

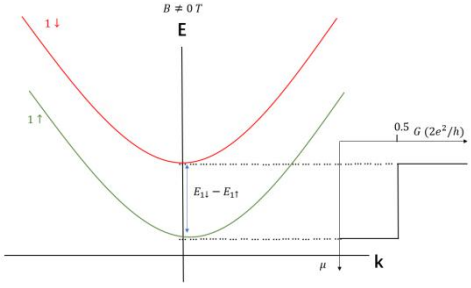
B ≠ 0 T
E
1↓
1↑
0.5
G (2e²/h)
E₁↓ − E₁↑
μ
k

f

Figure 4.4: Pinch-off traces of one device showing a quantized conductance plateau at 0.5 G_0 at high magnetic field. **a)** Conductance quantization as a function of gate voltage and perpendicular magnetic field at T= 1.7 K. **b)** Conductance quantization of the device for 8.0 T. Sweep forward (blue) and backward (orange) indicate low hysteresis of the semiconductor. **c)** Cross section view of InAsSb/Pb nanowire. It is measured with two probe method. By applying a small AC excitation voltage V_{AC} and then measuring the AC current I_{AC}. The conductance can be given by $\mathrm{G} = \frac{dI_{AC}}{dV_{AC}}$. **d)** SEM image of InAsSb/Pb shadow junction nanowire. **e)** shows the energy spectrum at zero magnetic field case. Each of two-spin degenerate sub-band below the Fermi level will result into a conductance of $\mathrm{G}_0 = \frac{2e^2}{h}$ when the chemical potential or the gate voltage reaches the lowest band. **f)** shows the energy spectrum at nonzero magnetic field case., the spin- degeneracy is lifted due to the Zeeman effect. It contributes to an energy spacing $\Delta\mathrm{E}_{\mathrm{subband}} = \mathrm{E}_{1\uparrow} - \mathrm{E}_{1\downarrow} = \mathrm{g}\mu_{\mathrm{B}}\mathrm{B}$ which will give a conductance of $\frac{e^2}{h}$ instead of $\frac{2e^2}{h}$.

4.3 Other discussions

In this section I will discuss various problems I was ever facing during this project. The results I got for these samples is not perfect due to several factors, but it will still provide a reference for the future experiments.

I.Problems to observe the superconductivity behaviour: possible type II superconductor

Other than normal superconducting phase., we also obverse some unusual properties shown in Figure 4.5a in certain device. This device shows two large critical temperatures H_{c1} and H_{c2} with two probe method, and the feature looks like a type II superconductor behaviour. The structure of Pb seems to have some change compared. Figure4.5b shows the upper critical field as function of temperature, and $H_{c2}(0)$ could be estimated to be 7.2 T. According to the Ginzburg-Landau theory for the upper critical field [48],

$$\mu_0 H_{c2} = \frac{h}{2e\zeta(0)^2}\frac{T_c - T}{T_c} \tag{4.1}$$

I can calcualte the Ginzburg-Landau coherence length $\zeta(0)$, which is 45.5 nm. It is smaller than common conherence length shown in the table 2.1 in Chapter 2 so that there is definitely possibility that it shows Type II superconductor behaviour. Since whether a superconductor belongs to a type I or to a type II material depends on the measurable Ginzburg Landau parameter [47],

$$\kappa = \frac{2\sqrt{2}\lambda_L{}^2(T)H_c(T)}{\phi_0}\left(1 + \frac{\zeta_0}{l}\right)\begin{cases} < 1/\sqrt{2}, & \text{Tpye I} \\ > 1/\sqrt{2}, & \text{Type II} \end{cases} \tag{4.2}$$

where ϕ_0 is magnetic flux quantum, λ_L is the London penetration depth, ζ_0 is Pippard coherence length, and l is mean free path. The Pb may be introduced some impurities such as In or Sb so that the mean free path of electrons l is reduced, and then increase this Ginzburg Landau parameter which result into a transition from type I superconductor to type II superconductor. What we measured on this device is not a pure Pb.

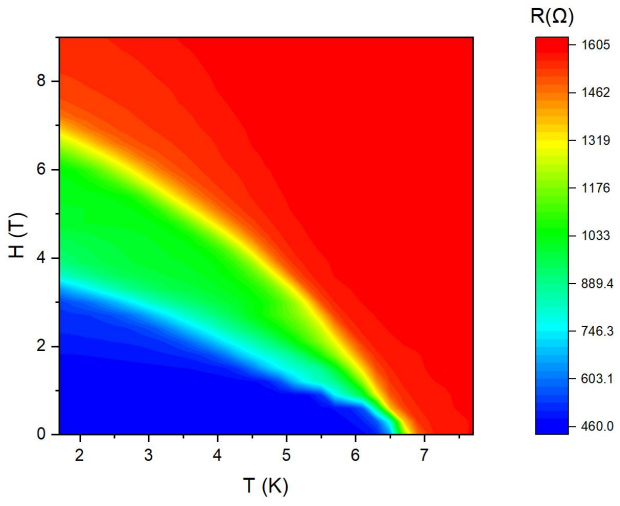

a

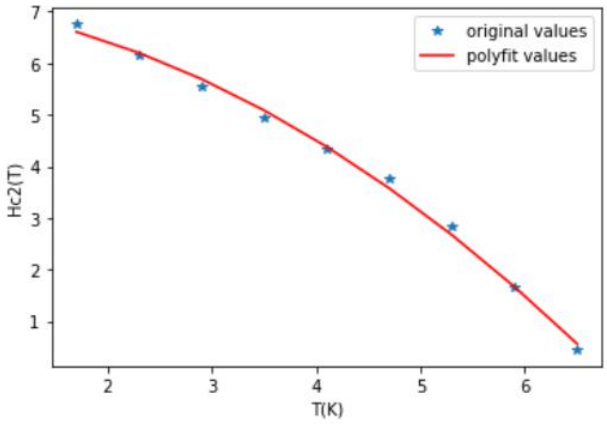

b

Figure.4.5: a). The thermodynamic phase diagram for one InSb/Pb VLS nanowire device (two probe measurement setup). Temperature sweeps from 1.7 K to 8 K, and magnetic field from 0 T to 9 T. The different transition lines shows type I and type II superconductor behaviour. **b)** Upper critical field as a function of T. $H_{c2}(0)$ could be estimated to be 7.2 T.

II.Problems to observe the pinch off behaviour

So far, I have only found one device that could show pinch of behaviour. The reason is probably due to the large thickness of Pb. Figure 4.6 shows the devices that have no pinch off behaviour observed.

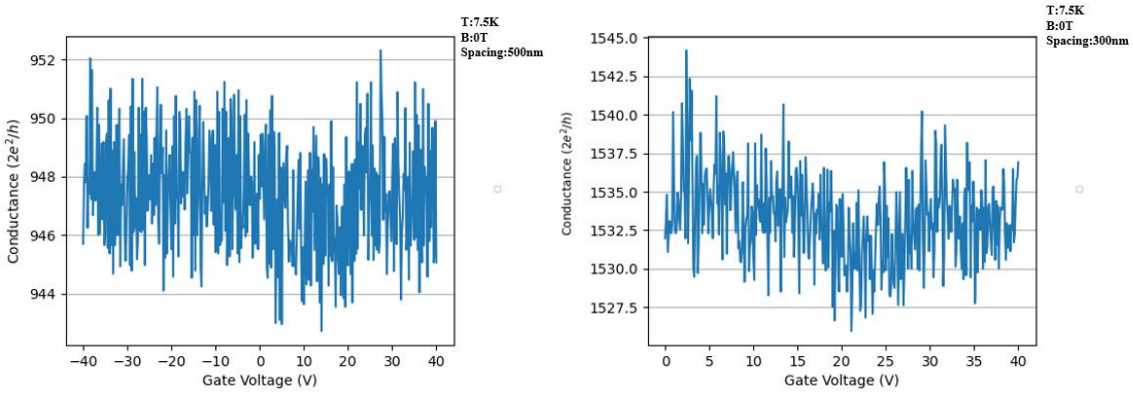

a **b**

Figure 4.6: Examples of devices that could not observe the pinch of behaviour. Due to the huge conductance of Pb, much noise induced by it will interrupt the observation of the gate dependent properties. Device (a) has the conductance of $948 \pm 4\ G_0$, and the device (b) has around $1535 \pm 10\ G_0$

In order to observe the pinch off behaviour, not only was I testing tons of devices but also trying to reduce the 1/f noise [45] as shown in Figure 4.7. The term 1/f noise is used broadly to refer to any noise whose power spectral density is inversely proportional to the frequency of the signal, $S(f) \propto 1/f^{\alpha}$, where α is typically $0<\alpha<2$, and f is the frequency. In the condensed matter devices, it is induced by the slow fluctuations. Sources of these fluctuations include defects in metals, and traps in semiconductors. In our experiment it is the frequency applying by the Lock-In amplifier. After many tests, I could find a clear pinch off curve at certain frequency.

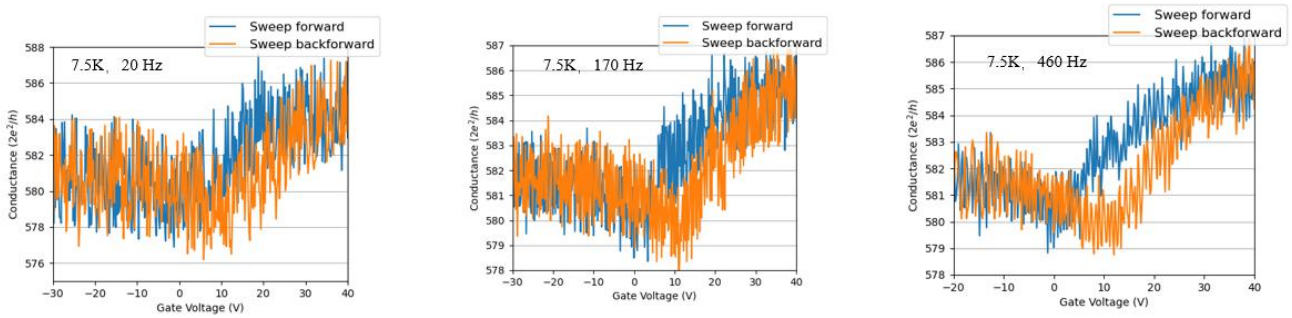

Figure 4.7: 1/f noise tests for different frequency.

Chapter 5 Conclusion and outlook

In this thesis, I presented my results of low temperature measurement experiments for the devices from InSb/Pb and InAsSb/Pb NWs. In this chapter, I am going to conclude the core outcomes from my thesis, associated with challenges.

Why hybrid materials and why Pb?

The Majorana zero modes are expected in a hybrid material of semiconductor nanowire with strong spin interaction and large g factor coupled with a superconductor. In order to observe it, the high crystal quality and disorder-free interface between the semiconductor and superconductor is important. Pb has the highest critical temperature and the highest critical magnetic field among all elemental type-I superconductors. It will provide a large induced superconducting energy gap so that it will be easy to observe Majorana zero modes. So far, Pb-based nanowires haven't been fully studied yet.

Key results

1. I developed device fabrication process for InSb/Pb or InAsSb/Pb NWs.
2. With the process, I obtained several chips with devices of InSb/Pb and InAsSb/Pb NWs.
3. With these devices, I found that Pb coupled with semiconductor nanowires show normal superconductivity with critical temperature (around 7.0 T) and critical magnetic field (around 1.14 T at 1.7 K). $H_c(0)$ is estimated to be 1.27 T.The devices of InSb/Pb without junctions also show pinch-off behavior and the devices of InAsSb/Pb could show quantized conductance at high magnetic fields.

Challenges and Next step

My work is an initial step of InSb/Pb NW study. There are a lot of work to be done in this interesting system. Based on my best knowledge, they are including:

1. Since we have got high-quality Pb-based nanowires with in-situ junctions, we would like to try the tunnel spectroscopy experiment to see if it could show hard gap superconductivity.
2. So far we can grow InSb/Pb nanowires with in-situ junction. However, to maximize the fabrication flexibility, the suitable etching process needs to be developed. The peracetic acid is probably an option.
3. The Pb layer on side facets of InSb nanowires needs to be thicker than that usually for Al. Otherwise, it will not be uniform. It could be possible to improve it, if the beam flux is high enough or the substrate is cold enough. Both can reduce the atom diffusion length and improve the uniformity. The effusion cell would keep the Pb flux stable while the Pb flux is high. The holder could have even lower temperatures with Helium cycling. Meanwhile, we have to oxide the Pb layer in the load lock, so the heat absorbed during transfer will also lead to dewetting of the Pb layer. The O_2 supply pipe or so-called Oxygen Atom Beam Source will stabilize the Pb layer without warming the sample up during unloading.

Bibliography

[1] Fisher, M. E. & Nagaosa, N. Profile of David J. Thouless, J. Michael Kosterlitz, and F. Duncan M. Haldane, 2016 Nobel Laureates in Physics. Proc. Natl Acad. Sci. USA 114, 626–628 (2017).

[2] Croom, Fred H. (1989), Principles of Topology, Saunders College Publishing, ISBN 978-0-03-029804-2

[3] Senthil T, Fisher MPA. Quasiparticle localization in superconductors with spin-orbit scattering. Phys Rev B 2000;61:9690-9698

[4] Moore, Joel E. (2010). "The birth of topological insulators". Nature. 464 (7286): 194–198. doi:10.1038/nature08916. ISSN 0028-0836. PMID 20220837. S2CID 191134

[5] Johnston, Hamish (23 July 2015). "Weyl fermions are spotted at long last". Physics World. Retrieved 22 November 2018.

[6] Majorana E, Maiani L. A symmetric theory of electrons and positrons. Ettore Majorana Scientific Papers. Springer, Berlin, Heidelberg, 2006: 201-233

[7] A. Yu. Kitaev, Annals of Physics 303, 2-30 (2003).

[8] Kitaev AY. Unpaired Majorana fermions in quantum wires. Physics-Uspekhi 2001;44:131-136.

[9] Fu L, Kane CL. Superconducting proximity effect and Majorana fermions at the surface of a topological Insulator. PhysRev Lett 2008;100:096407.

[10] Lutchyn, R., Bakkers, E.P.A.M., Kouwenhoven, L.P. et al. Majorana zero modes in superconductor–semiconductor heterostructures. Nat Rev Mater 3, 52–68 (2018). https://doi.org/10.1038/s41578-018-0003-1

[11] Nilsson H A, Caroff P, Thelander C, Larsson M, Wagner J B,Wernersson L-E, Samuelson L, Xu H Q 2009 Nano Lett. 93151

[12] Nilsson H A, Samuelsson P, Caroff P, Xu H Q 2012 NanoLett. 12 26

[13] Lee EJH, Jiang X, Aguado R, Katsaros G, Lieber CM, De Franceschi S. Zero-bias anomaly in a nanowire quantum dot coupled to superconductors. Phys Rev Lett 2012;109:186802.

[14] Pikulin DI, Dahlhaus JP, Wimmer M, Schomerus H, Beenakker CWJ. A zero-voltage conductance peak from weak antilocalization in a Majorana nanowire. New J Phys 2012;14:125011.

[15] Mourik V, Zuo K, Frolov SM, Plissard SR, Bakkers EP a.M, Kouwenhoven LP. Signatures of Majorana fermions in hybrid superconductor-semiconductor nanowire devices. Science 2012;338:1003-1007.

[16] Deng MT, Yu CL, Huang GY, Larsson M, Caroff P, Xu H Q. Anomalous zero-bias conductance peak in a Nb-InSb nanowire-Nb hybrid device. Nano Lett 2012;12:6414-6419.

[17] Das A, Ronen Y, Most Y, Oreg Y, Heiblum M, Shtrikman H. Zero-bias peaks and splitting in an Al-InAs nanowire topological superconductor as a signature of Majorana fermions. Nat Phys 2012;8:887-895.

[18] Churchill HOH, Fatemi V, Grove-Rasmussen K, Deng MT, Caroff P, Xu HQ, et al. Superconductor-nanowire devices from tunneling to the multichannel regime: Zero-bias oscillations and magnetoconductance crossover. Phys Rev B 2013;87:241401.

[19] Finck ADK, Van Harlingen DJ, Mohseni PK, Jung K, Li X. Anomalous modulation of a zero-bias peak in a hybrid nanowire-superconductor device. Phys Rev Lett 2013;110:126406.

[20] Deng MT, Yu CL, Huang GY, Larsson M, Caroff P, Xu H Q. Parity independence of the zero-bias conductance peak in a nanowire based topological superconductor-quantum dot hybrid device. Sci Rep 2014;4:7261.

[21] Krogstrup P, Ziino NLB, Chang W, Albrecht SM, Madsen MH, Johnson E, et al. Epitaxy of semiconductorsuperconductor nanowires. Nat Mater 2015;14:400-406.

[22] Chang, W., Albrecht, S., Jespersen, T. et al. Hard gap in epitaxial semiconductor–superconductor nanowires. Nature Nanotech 10, 232–236 (2015). https://doi.org/10.1038/nnano.2014.306

[23] Sabbir A. Khan, Charalampos Lampadaris, Ajuan Cui, Lukas Stampfer, Yu Liu, Sebastian J. Pauka, Martin E. Cachaza, Elisabetta M. Fiordaliso, Jung-Hyun Kang, Svetlana Korneychuk, Timo Mutas, Joachim E. Sestoft, Filip Krizek, Rawa Tanta, Maja C. Cassidy, Thomas S. Jespersen, and Peter Krogstrup ACS Nano 2020 14 (11), 14605-14615 DOI: 10.1021/acsnano.0c02979

[24] Jakob Kammhuber, Maja C. Cassidy, Hao Zhang, Önder Gül, Fei Pei, Michiel W. A. de Moor, Bas Nijholt, Kenji Watanabe, Takashi Taniguchi, Diana Car, Sébastien R. Plissard, Erik P. A. M. Bakkers, and Leo P. Kouwenhoven Nano Letters 2016 16 (6), 3482-3486 DOI: 10.1021/acs.nano lett.6b00051

[25] Gazibegovic, S., Car, D., Zhang, H. et al. Epitaxy of advanced nanowire quantum devices. Nature 548, 434–438 (2017). https://doi.org/10.1038/nature23468

[26] Zhang, H., Liu,CX., Gazibegovic, S.et al. RETRACTED ARTICLE: Quantized Majorana conductance. Nature 556, 74–79 (2018). https://doi.org/10.1038/nature26142

[27] Potts, H.; Friedl, M.; Amaduzzi, F.; Tang, K.; Tutuncuoglu, G.; Matteini, F.; Alarcon Llado, E.; McIntyre, P. C.; Fontcuberta i Morral, A. Nano letters 2015, 16, 637–643

[28] Sestoft JE, Kanne T, Gejl AN, von Soosten M, Yodh JS, Sherman D, et al. Engineering hybrid epitaxial InAsSb/Al nanowires for stronger topological protection. Phys Rev Mater 2018;2:044202.

[29] Vaitiekėnas, S., Liu, Y., Krogstrup, P. et al. Zero-bias peaks at zero magnetic field in ferromagnetic hybrid nanowires. Nat. Phys. 17, 43–47 (2021). https://doi.org/10.1038/s41567-020-1017-3

[30] Kanne, T., Marnauza, M., Olsteins, D. et al. Epitaxial Pb on InAs nanowires for quantum devices. Nat. Nanotechnol. 16, 776–781 (2021). https://doi.org/10.1038/s41565-021-00900-9

[31]Pendharkar M, Zhang B, Wu H, Zarassi A, Zhang P, Dempsey CP, et al. Parity-preserving and magnetic field resilient superconductivity in indium antimonide nanowires with tin shells arXiv 2019:1912.06071.

[32] Nadj-Perge, S. et al. Observation of majorana fermions in ferromagnetic atomic chains on a superconductor. Science 346, 602–607 (2014).

[33] Wang, Dongfei, Kong, Lingyuan, Fan, Peng, Chen, Hui, Zhu, Shiyu, Liu, Wenyao, Cao, Lu, Sun, Yujie, Du, Shixuan, Schneeloch, John, Zhong, Ruidan, Gu, Genda, Fu, Liang, Ding, Hong, and Gao, Hong-Jun. Evidence for Majorana bound states in an iron-based superconductor. United States: N. p., 2018. Web. https://doi.org/10.1126/science.aao1797.

[34] Tinkham, M. (1996). Introduction to Superconductivity, Second Edition. New York, NY: McGraw-Hill. ISBN 0486435032.)

[35] Bardeen, J. (March 1955). "Theory of the Meissner Effect in Superconductors". Physical Review. 97 (6): 1724–1725 doi:10.1103/PhysRev.97.1724

[36] London, F. (September 1948). "On the Problem of the Molecular Theory of Superconductivity". Physical Review. 74 (5): 562–573. doi:10.1103/PhysRev.74.562

[37] Ginzburg VL (July 2004). "On superconductivity and superfluidity (what I have and have not managed to do), as well as on the 'physical minimum' at the beginning of the 21 st century". ChemPhysChem. 5 (7): 930–945. doi:10.1002/cphc.200400182. PMID 15298379

[38] Bardeen, J.; Cooper, L. N.; Schrieffer, J. R. (December 1957). "Theory of Superconductivity". Physical Review. 108 (5): 1175–1204. doi:10.1103/PhysRev.108.1175

[39] Chuancheng Jia et al. “Nanowire Electronics : From Nanoscale to Macroscale”. In: (2019). DOI: 10.1021/acs.chemrev.9b00164

[40] Essick, J. (2007). An Examination of Quantized Conductance in Nanowires. Retrieved August 24, 2021

[41] Krogstrup, P.; Ziino, N. L. B.; Chang, W.; Albrecht, S. M.; Madsen, M. H.; Johnson, E.; Nygard, J.; Marcus, C. M.; Jespersen, T. S. Nat. Mater. 2015, 14, (4), 400-406.

[42] Quantum Design. “Physical Property Measurement System, DynaCool User’s Manual”. In: 1307 (2011).

[43] Tinkham, M. (1996). Introduction to Superconductivity, Second Edition. New York, NY: McGraw-Hill. ISBN 0486435032.

[44] Eisenstein, J. (1954). "Superconducting Elements". Reviews of Modern Physics. 26 (3): 277–291.

[45] Kogan, Shulim (1996). Electronic Noise and Fluctuations in Solids. [Cambridge University Press]. ISBN 978-0-521-46034-7.

[46] Fadaly E M T, Zhang H, Conesa-Boj S, Car D, Gül Ö,Plissard S R, Op Het Veld R L M, Kölling S,Kouwenhoven L P and Bakkers E P A M 2017 Observation of conductance quantization in InSb nanowire networks Nano Lett. 17 6511 – 5

[47] Boersch, H. Kunze, U. Lischke, B. & Rodewald, W. (1973). Observation of the mixed state in films of type I superconductors (Pb). Physics Letters A, 44, 273-274.

[48] Superconductivity, Superfluids, and Condensates (Oxford Master Series in Conden Item Condition: New. Published On: 2005-08-11 SKU: 4444-GRD-9780198507567.